NCAR/TN-???+STR
DRAFT ..... NCAR TECHNICAL NOTE

19 February 2010

An Overflow Parameterization for the Ocean Component of the Community Climate System Model

B. P. Briegleb, G. Danabasoglu and W. G. Large

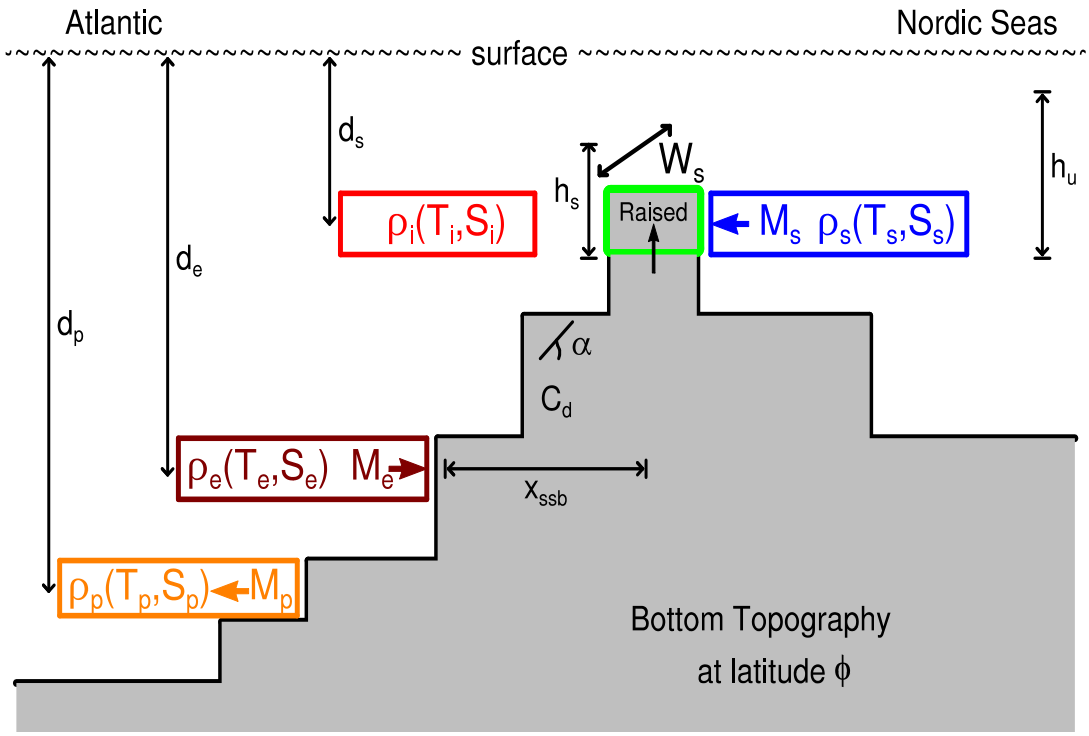

CLIMATE AND GLOBAL DYNAMICS DIVISION

NATIONAL CENTER FOR ATMOSPHERIC RESEARCH
BOULDER, COLORADO

AN OVERFLOW PARAMETERIZATION FOR THE OCEAN COMPONENT OF THE COMMUNITY CLIMATE SYSTEM MODEL

by Bruce P. Briegleb, Gokhan Danabasoglu and William G. Large

National Center for Atmospheric Research

P.O. Box 3000, Boulder, CO 80307

TABLE OF CONTENTS

Abstract

The Overflow Parameterization (OFP) for the ocean component of the Community Climate System Model (CCSM) is presented. The ocean component is based on the Parallel Ocean Program Version 2, or POP2, of the Los Alamos National Laboratory (Smith et al., 2010). The OFP has two parts: the method of evaluating overflow properties based on ocean model state, and the modifications to the baroclinic and barotropic solutions to reflect the influence of the overflows.

Evaluating overflow properties involves computing source water transport based on regional averages over an interior and source domain. The source overflow is implemented as a sidewall boundary condition on raised bottom topography, which replaces explicitly resolved overflow with the parameterized overflow. The parameterized overflow is assumed to flow through the ridge (implicitly) and to descend unmodified to an entrainment sidewall, where entrainment ambient water is mixed with the source water, producing the final product water. The product density is computed for the mix of source and entrainment waters, and the product injection position is found where neutral buoyancy occurs along a pre-specified product path.

In POP2 the baroclinic and barotropic modes are split. Our approach is to solve the baroclinic equations without change but to modify the barotropic equation to include the effect of the parameterized overflows. We assume that the overflow sidewall velocities are total velocities at each time step, and this non-zero sidewall boundary condition is used to modify the barotropic continuity equation, as well as the vertical planar column velocities above each sidewall at source, entrainment and product locations so that local mass conservation is enforced. Overflow tracer advection is done through the source, entrainment and product sidewalls in a conservative manner.

The POP2 implementation allows the user to select overflow source, entrainment and product locations and orientations. It allows for more than one product location so that the product depth can adjust to varying forcing. Various parameters can be adjusted, ideally within observational constraints, to yield overflow transports within observational uncertainties. The implementation method should be applicable to z-coordinate ocean models with the baroclinic/barotropic split as in POP2.

1. Introduction to the Overflow Parameterization (OFP)

Oceanic overflows, also known as gravity currents, are flows of dense waters formed in marginal seas and on coastal shelves. These dense waters become the source for gravity current overflows, which flow through narrow canyons or over sills, entraining ambient waters as they descend down continental slopes to finally form deep interior oceanic waters. It is thought that oceanic overflows are important to the formation of deep bottom waters and thus play an important role in the oceanic thermohaline circulation (Dickson and Brown, 1994, Dye et al. 2007, Legg et al. 2009). Important overflows are the Nordic Sea overflows (Denmark Strait and Faroe Bank Channel) and the Antarctic overflows (Ross Sea and Weddell Sea).

Representing overflows in global ocean components used in coupled climate models is not directly possible because of the small scale of the flows, both horizontally and vertically (Girton et al. 2006, Dye et al. 2007, Macrander er al. 2007). The flows are often constrained by canyons or bottom topographic features to be order ten to a few hundred km in horizontal scale, and as they are bottom boundary layer flows their vertical scale is order a few hundred meters thick. Typical oceanic horizontal length scales in coupled climate models are order 100 km, while many such models employ a vertical z-coordinate with layer thickness order 100-200 m. Additionally, flow down stair-step topography in z-coordinate models is known to be excessively entraining with ambient waters, making descent of dense waters unmixed with ambient to the deepest possible level difficult (Roberts et al. 1996, Winton et al. 1998, Griffies et al. 2000, Bryan et al. 2006).

Attempts to date to represent overflows in coarse resolution ocean models have had limited success. Both Kosters et al. (2005) and Born et al. (2008) employed hydraulic transport in the Denmark Strait in very coarse ocean models but still had poor representation of the entrainment and the descent of the product plume, and an overflow transport through the straight required for realistic North Atlantic circulation was about twice observed ($\approx$6 Sv). Artificially widening and deepening the Greenland-Iceland-Scotland (GIS) ridge is an ad-hoc approach which Roberts and Wood (1997) show results in quite large model solution sensitivity to small changes in bottom topography. Using high resolution nested grids poses technical challenges in coupling with the global ocean model. Sloped or partial bottom cells do not appear to improve overflows in steep-sloped regions (Griffies et al. 2000).

An attractive way to represent sub-grid scale overflows in z-coordinate ocean models is to parameterize them based on the resolved density and topographic features. One such parameterization is that of Price and Yang (1998). Based on a simple model with several observed parameters, the overflow transport can be computed with input density differences between interior and source regions. Using the method of Price and Baringer (1994) further allows the entrainment of ambient downstream waters based on density differences between source and entrainment regions. The final product water is then injected down-

stream where neutral buoyancy is achieved. High resolution process model studies support such parametric efforts (Riemenschneider and Legg, 2007). Wu et al. (2007) show how a special case of this parametric approach was applied successfully to the Mediterranean overflow.

To apply this parameterization in an ocean model requires a way to ensure numerical stability in flow fields and tracer conservation during overflow transport. Here we apply an overflow parameterization to POP2, a z-coordinate ocean model with a baroclinic/barotropic mode split (Smith et al., 2010). We call this representation of overflows the Overflow Parameterization (OFP). We employ a topographic sidewall velocity appropriate for overflow transport at three distinct locations: source, entrainment and product. For the source, we raise (or pop-up) the bottom topography to replace the explicitly resolved overflow with the parameterized one. For numerical stability it was necessary to enforce local mass conservation but allow tracer transport through the side walls in a conserving manner. In effect, the flow between source to entrainment, and entrainment to product, is implicit. Allowing for a number of product injection points of increasing depth results in a dynamic overflow product level to varying forcing. This approach is a generalization of the overflow parameterization used by Wu et al. (2007) for POP1.4 .

This technical report presents the OFP continuous equations, discrete equations, and the implementation into POP2. It includes appendices which present the derivation of the OFP equations, application to observations, and a brief dicsussion of OFP code, input file and restart file. Included are appendices with the POP2 vertical grid and a glossary of acronyms.

2. Continuous Equations

2A. For Ocean Model State

Here we present the continuous equations of OFP related to the ocean model state. We follow Whitehead et al. (1974), Price and Yang (1998), and Price and Baringer (1994). A detailed derivation of the OFP equations is given in Appendix A, while an application of the equations to real overflows using observed inputs is given in Appendix B.

We assume a marginal sea is connected to the open ocean by a channel (sometimes referred to as a canyon, sill or straight) at latitude ϕ, where the channel floor is assumed to be elevated compared to the open ocean and marginal sea basins on either side, and has a rectangular geometry of depth d_s (from the surface) and width W_s. We assume that the channel width W_s is larger than the Rossby radius of deformation (see Appendices A and B for further discussion). On the marginal sea side is a source water region, with temperature, salinity and associated density T_s, S_s and ρ_s respectively at the sill depth d_s. The thickness of this source region from the depth of the sill upwards is h_u, where $h_u < d_s$. On the ocean side of the channel is an interior region with temperature, salinity and

associated density T_i, S_i and ρ_i respectively at depth d_s. If $\rho_s > \rho_i$, then source waters flow from the marginal sea through the channel and into the open ocean. The open ocean has a continental shelf away from the channel exit which extends to a shelf-slope break, with the maximum bottom slope near the shelf-slope break characterized by α and the distance from channel to shelf-slope break x_{ssb}. The overflow is assumed to spread laterally over the bottom during descent along the continental shelf due to bottom friction, characterized by a constant drag coefficient C_d. At the shelf slope break is an entrainment region with temperature, salinity and associated density T_e, S_e and ρ_e respectively at depth d_e. If the source water density at depth d_e is greater than ρ_e, then entrainment may occur of amount dependent on the flow and shelf slope parameters just mentioned. The mixed source and entrainment waters are assumed to descend as product water down a predefined path until neutral density is reached at depth d_p.

Table 1 gives a summary of the overflow parameters. Six input parameters must be specified (h_u and h_s are related as in Eq. 4 below), along with regions for which ocean properties of temperature, salinity and depth are available: interior, source, entrainment, and one or more product injection depths. From these regions the corresponding ocean density can be evaluated. The interior region is assumed to be in the open ocean but close to the channel, the source region is in the marginal sea near the channel, while the entrainment region is at depth near the continental shelf-slope break on the open ocean side. Additionally, there are various product injection depths downstream in the open ocean where overflow product waters may flow. The product path is the connection of the product injection depths ordered by increasing depth. (See Sections 4B and 4C).

Figure 1 gives a schematic of the overflow parameterization parallel to the flow from source to product. All of the overflow parameters listed in Table 1 are shown in Figure 1. Note how the parameterization assumes a raised (or "popped-up") topography between the interior and source region (the green box in Fig.1). By using this raised topography, the OFP significantly reduces resolved overflow from a model without parameterized overflows and substitutes the overflow parameterization instead.

For the source transport (the blue arrow in Fig. 1), we follow Whitehead et al. (1974) who considered a two-layer rotating, hydrostatic, inviscid fluid filling a channel connecting two basins. The two fluids are represented in Fig. 1 by the source (T_s, S_s; blue box in Fig. 1) and interior (T_i, S_i; red box in Fig. 1) temperature and salinities respectively, and the corresponding densities:

$$\begin{aligned} \rho_s &= \rho(T_s, S_s, d_s) \\ \rho_i &= \rho(T_i, S_i, d_s) \end{aligned} \tag{1}$$

where $\rho(T, S, d)$ is the ocean density for temperature T, salinity S, and depth d, and we evaluate these densities at the channel depth d_s. The density difference between these two fluids in the channel drives a steady geostrophic flow through the straight.

Table 1. Summary of Overflow Parameters. Interior, source and entainment regions refer to specified three-dimensional volumes within the ocean. These are rectangular latitude/longitude areas at a specified ocean depth. (see Table 3). Product injection depths have predetermined locations (see Table 4).

Symbol	Description	Units
	Parameters	
ϕ	latitude of overflow	degrees
W_s	width of straight	km
h_u	upstream thickness of the source water	m
h_s	source thickness in the channel	m
x_{ssb}	distance from sill to shelf-slope break (ssb)	km
α	maximum bottom slope near shelf-slope break	none
C_d	bottom shelf drag coefficient	none
	Interior Region	
d_s	interior region depth	m
T_i	interior region temperature	$^\circ$C
S_i	interior region salinity	psu
ρ_i	ocean density from interior T_i,S_i,d_s	kg m^{-3}
	Source Region	
d_s	source region depth	m
T_s	source region temperature	$^\circ$C
S_s	source region salinity	psu
ρ_s	ocean density from source T_s,S_s,d_s	kg m^{-3}
	Entrainment Region	
d_e	entrainment region depth	m
T_e	entrainment region temperature	$^\circ$C
S_e	entrainment region salinity	psu
ρ_e	ocean density from entrainment T_e,S_e,d_e	kg m^{-3}
	One or more Product Injection Depths	
d_p	various product depths	m
T_p	product temperature	$^\circ$C
S_p	product salinity	psu
ρ_p	product ocean density for various d_p	kg m^{-3}

The density difference in the channel specifies the source reduced gravity g'_s, written as:

$$g'_s = \frac{\rho_s - \rho_i}{\rho_0} g \tag{2}$$

where g is the acceleration of gravity, $\rho_0 = 1027$ kg m^{-3} is a reference ocean density. As long as $g'_s > 0$ source overflow transport will occur. Assuming the straight width is larger than the Rossby radius of deformation, and that regional geometry allows inflow over a much larger region than the straight, the maximal geostrophic transport through the staight for a hydraulically controlled flow is given by:

$$M_s = \frac{g'_s h_u^2}{2f} = \frac{9}{8} \frac{g'_s h_s^2}{f} \tag{3}$$

where the Coriolis parameter is $f = 2\Omega_e \ sin(\phi)$, Ω_e is Earth's angular velocity, ϕ is the latitude, h_u is the upstream thickness of the source waters, and h_s is the source thickness of overflow waters in the channel connecting the marginal sea and the ocean, given by:

$$h_s = \frac{2}{3} h_u \ . \tag{4}$$

Assuming a rectangular cross sectional area $A_s = h_s W_s$, an associated source speed U_s can be evaluated:

$$U_s = \frac{M_s}{A_s} \ . \tag{5}$$

Thus we assume the source overflow exits the channel with volume transport M_s, with a rectangular geometry of width W_s, height h_s and speed U_s. Following Price and Baringer (1994), we assume the source overflow forms a descending, widening and thinning bottom gravity current that flows unmixed down the shelf to the shelf-slope break, where entrainment with ambient fluid of properties (T_e, S_e) may occur (brown box in Fig. 1). Such mixing at the shelf-slope break can occur if the geostrophic Froude number F_{geo} is greater than 1:

$$F_{geo} = U_{ssb} / \sqrt{g'_e h_{ssb}} \tag{6}$$

where U_{ssb} is the flow speed and h_{ssb} is the flow thickness of the overflow gravity current at the shelf-slope break, and g'_e is an entrainment reduced gravity given by:

$$g'_e = \frac{\rho'_s - \rho_e}{\rho_0} g \tag{7}$$

where

$$\begin{aligned} \rho'_s &= \rho(T_s, S_s, d_e) \\ \rho_e &= \rho(T_e, S_e, d_e) \end{aligned} \tag{8}$$

with ρ'_s the source water density at the entrainment depth d_e, and ρ_e the entrainment region density. The flow speed at the shelf-slope break is assumed to result from a geostrophic balance between the slope and Coriolis accelerations:

$$U_{ssb} = \frac{g'_e \alpha}{f} \tag{9}$$

where α is the maximum bottom slope near the shelf-slope break. The overflow thickness at the shelf-slope break, by volume conservation of the flow exiting the channel, is:

$$h_{ssb} = \frac{U_s h_s W_s}{U_{ssb} W_{ssb}} \tag{10}$$

where spreading width W increases linearly with distance from the source. We assume that the descending gravity current between the channel exit and the shelf-slope break widens and thins due to a near geostrophic balance between the slope acceleration and Coriolis acceleration, but with some bottom drag. Thus we represent the gravity current width between the channel exit and the shelf-slope break as $W(x) = W_s + 2Kx$, where x = the distance from the channel exit, such that at the shelf-slope break:

$$W_{ssb} = W_s + 2Kx_{ssb} \tag{11}$$

with the Ekman number K specified by the balance between bottom drag over the mean thickness of the overflow $(1/2(h_s + h_{ssb}))$ and Coriolis force:

$$K = \frac{C_d U_{avg}}{1/2(h_s + h_{ssb})f} \tag{12}$$

with C_d the bottom drag coefficient, and the average flow speed during spreading is:

$$U_{avg} = 1/2(U_s + U_{ssb}) \ . \tag{13}$$

Eqs. 10-12 can be solved simultaneously for h_{ssb}, which then allows evaluation of all the remaining parameters. So long as the geostrophic Froude number $F_{geo} > 1$, then an entrainment mixing parameter ϑ can be evaluated:

$$\vartheta = \frac{M_e}{(M_s + M_e)} = 1 - F_{geo}^{-2/3} \tag{14}$$

which is the fraction of the entrainment volume transport compared to the total $M_s + M_e$. If $g'_e \leq 0$ or if $F_{geo} \leq 1$, ϑ is set to 0. The entrainment volume transport is:

$$M_e = M_s \frac{\vartheta}{(1 - \vartheta)} \ . \tag{15}$$

The product (p) volume transport M_p is then:

$$M_p = M_s + M_e \ . \tag{16}$$

The product water temperature T_p and salinity S_p are given by:

$$\begin{aligned} T_p &= T_s(1 - \vartheta) + T_e\vartheta \\ S_p &= S_s(1 - \vartheta) + S_e\vartheta. \end{aligned} \tag{17}$$

Eqs 16 and 17 ensure mass and tracer conservation respectively.

The product density $\rho_p(T_p, S_p, d_p)$ is evaluated along the product path for increasing depth d_p. Let N_p be the number of pre-determined product sites ($N_p > 1$) ordered by increasing depth d_p. The ambient density is computed from volume-averaged T and S adjacent to the product sites. The deepest possible product site is determined as follows. Starting with the deepest site N_p, if $\rho_p(T_p, S_p, d_p^{N_p-1})$ is larger than the $N_p - 1$ ambient density, the product level is at depth $d_p^{N_p}$, and if not, the next higher level is checked. If $\rho_p(T_p, S_p, d_p)$ is less than all product ambient densities, the shallowest site is chosen. Note that the ambient ocean density along the product path is not necessarily monotonically increasing, since the product path extends horizontally as it deepens. (See section 4C for a description of product paths as implemented in POP2). The product injection site is shown schematically in Fig. 1 as the orange box.

2B. For Ocean Model Baroclinic/Barotropic Solutions

The overflow volume transports are applied as topographic sidewall velocity boundary conditions, for source, entrainment and product separately ($u_{ovf} = M_s/A_s, M_e/A_e, M_p/A_p$ where A_s, A_e, A_p are the sidewall facial areas- note that A_s here is distinct from that in Eq. 5). For each location it is assumed that the total sidewall velocity is due to the overflow (i.e. u_{ovf}). This requires an adjustment of the velocity column above the sidewall to be consistent with the definitions of the baroclinic and barotropic velocities. In effect, mass conservation is ensured by this column adjustment for the active column into or out of which overflow occurs. Similarly, the adjacent column above topography which has overflow into it must have the vertical integral of the continuity equation (which is used in the derivation of the linearized barotropic continuity equation, see Smith et al. 2010) extended to the level of the overflow. This extension results in an extrae forcing term in the barotropic equation which ensures mass conservation in this column. Thus, local mass conservation is satisfied while the sidewall overflows transport tracers from source and entrainment regions to the product injection depth. Now we elaborate on this summary.

In an ocean model with a baroclinic/barotropic split, the total horizontal velocity u is given by:

$$u = u' + U \tag{18}$$

where u' is the baroclinic velocity and U is the barotropic velocity. For the barotropic and baroclinic velocities we have:

$$\begin{aligned} U &= \frac{1}{H+\eta}\int_{-H}^{\eta} u \; dz \\ \frac{1}{H+\eta}\int_{-H}^{\eta} u' dz &= 0 \end{aligned} \tag{19}$$

where z is the vertical coordinate positive upward, η is the free surface displacement relative to $z = 0$, and H is the ocean depth relative to $z = 0$ for velocity points.

For those columns where overflows occur, the integral and the normalization depth H must be extended downwards to the level of the overflow. The baroclinic and barotropic velocities are assumed valid over the entire column $H' = H+\Delta z_a+\Delta z_o$, where Δz_a is the depth of the sidewall above the overflow, and Δz_o is the depth of the sidewall at the overflow. (If the level of the overflow is the first below the top of the topography, the depth $\Delta z_a = 0$.)

For the barotropic velocity, the extension downward for overflow columns is accomplished by increasing H to the overflow level in the barotropic equations. For the barotropic continuity equation, the extension downwards must be into any column with an overflow sidewall, which modifies the horizontal divergence term in the vertical integral. This can be illustrated by taking the vertical integral of the continuity equation $\nabla \cdot u + \frac{\partial w}{\partial z} = 0$ for such a column:

$$\int_{-H-\Delta z_a-\Delta z_o}^{\eta} (\nabla \cdot u)\ dz + w(\eta) - w(-H - \Delta z_a - \Delta z_o) = 0 \tag{20}$$

where w is the vertical velocity. The integral term can be written as three separate terms:

$$\int_{-H-\Delta z_a-\Delta z_o}^{\eta} (\nabla \cdot u)\ dz = \int_{-H}^{\eta} (\nabla \cdot u)\ dz + \int_{-H-\Delta z_a}^{-H} (\nabla \cdot u)\ dz + \int_{-H-\Delta z_a-\Delta z_o}^{-H-\Delta z_a} (\nabla \cdot u)\ dz \tag{21}$$

The first term is the usual integral above the topopgraphy, the second term vanishes because total velocity is zero on the sidewalls above the overflow (if any), but the third term is non-zero, and for the illustrative case of an east-west oriented overflow, can be written:

$$\begin{aligned} \int_{-H-\Delta z_a-\Delta z_o}^{-H-\Delta z_a} (\nabla \cdot u)\ dz &= (\frac{U_E - U_W}{\Delta x})\Delta z_o \\ &= -\frac{u_{ovf}}{\Delta x \Delta y}\Delta y \Delta z_o \\ &= -\frac{M}{\Delta x \Delta y} \end{aligned} \tag{22}$$

where $U_E,\ U_W$ are the east and west face velocities, respectively, for a box of longitudinal width Δx and meridional width Δy, and we consider the case of an overflow on the east face, with $U_W = 0$, $U_E = -u_{ovf}$, where u_{ovf} is the overflow velocity and $M = u_{ovf}\Delta y \Delta z_o$ is the overflow volume transport through the sidewall area of $\Delta y \Delta z_o$. We can interpret the right-hand-side term above as follows. From the derivation of the linearized barotropic continuity equation in Smith et al. (2010), we have

$$w(\eta) = \frac{\partial}{\partial t}\eta - q_w \tag{23}$$

where η is the free surface height and q_w is the surface fresh water flux from land runoff, sea ice formation and melt, and net atmospheric water exchange. Thus, we can write the vertical integral of the continuity equation for this column as:

$$\frac{\partial}{\partial t}\eta = -\int_{-H}^{\eta} (\nabla \cdot u)\ dz + w(-H - \Delta z_a - \Delta z_o) + q_w + \frac{M}{\Delta x \Delta y} \tag{24}$$

where now the explicit overflow source term ensures continuity in this column. Let the resulting barotropic velocity using this modified forcing be U.

For the baroclinic velocity (Eq 19), let u'^* be the unnormalized baroclinic velocity from the solution to the baroclinic momentum equations for which the original depth $-H$ is used for all overflow columns. Above the overflow the sidewall velocity boundary condition is $u = 0$, implying that $u' = -U$. At the level of the overflow, we have $u' = u_{ovf} - U$. With u' known down to the level of the overflow along the sidewall, we extend the above baroclinic integral in Eq. 19 to include the increased depth, as:

$$\frac{1}{H + \eta + \Delta z_a + \Delta z_o} \int_{-H-\Delta z_a-\Delta z_o}^{\eta} u' dz = 0 \tag{25}$$

Separating this integral into three parts, using the definition of normalized $u' = u'^* - \bar{u}'^*$, where $\bar{u}'^*$ is the extended vertical normalization integral for u'^* (i.e. Eq 19 extended to the overflow level) and noting the normalization factor $H + \eta + \Delta z_a + \Delta z_o$ is ignorable, yields:

$$\begin{aligned}
&\frac{1}{H + \eta + \Delta z_a + \Delta z_o}\{\int_{-H}^{\eta} u' \; dz \; + \int_{-H-\Delta z_a}^{-H} u' \; dz \; + \int_{-H-\Delta z_a-\Delta z_o}^{-H-\Delta z_a} u' \; dz\} = 0 \\
&\frac{1}{H + \eta + \Delta z_a + \Delta z_o}\{\int_{-H}^{\eta} (u'^* - \bar{u}'^*) \; dz \; - U \; \Delta z_a \; + (u_{ovf} - U) \; \Delta z_o\} = 0 \\
&\qquad\qquad\qquad\qquad\qquad\qquad\qquad\qquad\qquad\qquad\qquad\qquad or \\
&\qquad\qquad\qquad\qquad\qquad\qquad H \; \bar{u}'^* - \int_{-H}^{\eta} u'^* \; dz = (u_{ovf} - U) \; \Delta z_o \; - U \; \Delta z_a \\
&\qquad\qquad\qquad\qquad\qquad \bar{u}'^* = \frac{1}{H}\{(u_{ovf} - U) \; \Delta z_o - \; U \; \Delta z_a + \int_{-H}^{\eta} u'^* dz\} \\
&\qquad\qquad\qquad\qquad\qquad\qquad\qquad u' = u'^* - \bar{u}'^*
\end{aligned} \tag{26}$$

Thus, we renormalize the baroclinic velocity for an overflow column using the next-to-the-last two equations in Eq. 26. This results in local mass conservation and consistency between the overflow sidewall velocity $u_{ovf} = M/(\Delta y \Delta z_o)$, the overflow column above it with $u' = u'^* - \bar{u}'^*$, and with the adjacent column over the topography where U was solved using the overflow forcing $M/(\Delta x \Delta y)$.

Tracer transport must include the sidewall overflow volume transports. For example, transport of temperature into the ocean domain at source, entrainment and product sidewalls would be $-M_s T_s$, $-M_e T_e$, and $+M_p T_p$ respectively, so that tracer conservation for temperature is satisfied, since

$$M_p T_p = M_s T_s + M_e T_e \tag{27}$$

from Eqs. 14-17.

Table 2 shows the overflow modifications to the POP time stepping scheme summarizing the above discussion. Note from this table that the overflow regional tracers advected in part (2) of the table are time-lagged with respect to the present time step, i.e. if n is the present time step index and $n+1$ is to be evaluated as in the table, then the overflow tracer values are at time step n (from the previous step), while the final tracer values are at time step $n + 1$.

Table 2. Overflow modifications to the POP2 time stepping scheme. Normal evaluations on the left side of the table; *Overflow Modification* denotes a OFP change, with a description given on the right hand side. See Smith et al. (2010).

(1) Evaluate Forcing and Coefficients	
Penetrative solar heating, vertical diffusivities and viscosities, horizontal viscosities including GM and anisotropic contributions.	
(2) Evaluate Predictor Θ and S	
Overflow Modification	Modify $\pounds_T(\Theta)$ and $\pounds_T(S)$ to include sidewall overflow tracer transport
$(1+\xi)\frac{\partial\hat{\Theta}}{\partial t} = -\pounds_T(\Theta) + D_H(\Theta) + D_V(\Theta) + Q_{SW}$	
$(1+\xi)\frac{\partial\hat{S}}{\partial t} = -\pounds_T(S) + D_H(S) + D_V(S)$	
(3) Update Pressure	
$p = p_s + p_h$	
(4) Solve Baroclinic Momentum Equations and Normalize $\vec{u}'$	
$\frac{\partial\vec{u}'^*}{\partial t} = f\hat{z}\times\vec{u} - \pounds_U(\vec{u}) - \frac{1}{\rho_0}\nabla p_h + F_H(\vec{u}) + F_V(\vec{u})$	
Overflow Modification	Save $\vec{u}'^*$ for overflow columns
$\vec{u}' = \vec{u}'^* - \frac{1}{H}\int_{-H}^{0}\vec{u}'^* dz$	
Overflow Modification	Calculate regional T, S and overflow transports M_s, M_e, M_p
(5) Solve Barotropic Equations and Update Total Velocity	
Overflow Modification	Evaluate overflow forcing term $F_{ovf} = (-M_s,\ -M_e,\ +M_p)/A_{(i,j)}$ Modify H for overflow columns
$\frac{\partial\vec{U}}{\partial t} = f\hat{z}\times\vec{U} - g\nabla\eta + \vec{F}_B$	
Overflow Modification	Include F_{ovf} in barotropic continuity equation
$\frac{\partial\eta}{\partial t} = -\nabla\cdot H\vec{U} + q_w + F_{ovf}$	
Overflow Modification	Renormalize overflow columns so $u' = u'^* - \bar{u}'^*$ $v' = v'^* - \bar{v}'^*$
$\vec{u} = \vec{u}' + \vec{U}$	
(6) Correct Tracers Θ and S	
$(1+\tilde{\xi})\frac{\partial\Theta}{\partial t} = F_{c\Theta}$	
$(1+\tilde{\xi})\frac{\partial S}{\partial t} = F_{cS}$	

3. Discretized Equations

POP2 is a z-coordinate ocean model with a baroclinic/barotropic split. It uses an Arakawa-B spatial discretization, where tracers (such as temperature and salinity) are referenced to a "tracer", or T-grid, while the xy components of velocity (u, v) are referenced to a "U", or U-grid on the corners of a T-grid box at the same vertical level. Typical nomenclature refers to a particular T-grid box via (i, j, k) indices, which correspond to the xyz coordinates. Unless otherwise indicated, a reference to (i, j, k) implies T-grid indices. U-grid indices refer to the northeast corner of a T-grid box (increasing x is "east" and increasing y is "north"), see Fig. 2. The vertical index k (or level) refers to the T-grid box, with k increasing downwards (see Table C1). Bottom topography is represented for each column by a maximum value of k, usually referred to as "kmt", i.e. for a given (i, j) ocean location, $k = kmt(i, j)$ is the deepest active ocean T-grid box above the bottom topography. Sidewall boundary conditions are zero normal and tangential velocities, i.e. $(u, v) = 0$ along a sidewall. Vertical velocity w is diagnosed from the continuity equation assuming zero flow through the bottom topography as well as side-walls.

The discretization of OFP has two parts: evaluation of overflow properties based on ocean model state, and the modifications to the baroclinic and barotropic solutions to reflect the influence of the overflows.

3A. For Ocean Model State

Consider the src (see Appendix G) region first. At the location of the source overflow in the model, we raise up at least three (more are possible) adjacent T-grid boxes by reducing their kmt by 1. The rationale' for this is to replace the original resolved overflow at this level with the parameterized overflow. In the direction of the overflow we impose an overflow velocity (u or v depending on orientation) on the sidewall of these raised boxes as a total velocity. In Fig. 1 the raised (or popped-up) topography is at the same level as the src and int regions.

To illustrate, let there be three adjacent T-grid boxes denoted by $(i, j-1, k), (i, j, k), (i, j+1, k)$ so that the overflow direction is "east-west" in grid space (i.e. the three adjacent grid boxes run "north-south"), as in Fig. 2. These three indices refer to grid boxes within the topography, so that the overflow level k satisfies $k = kmt(i, j-1) + 1 = kmt(i, j) + 1 = kmt(i, j+1) + 1$. The three adjacent grid boxes $(i+1, j-1, k), (i+1, j, k), (i+1, j+1, k)$ are all active ocean T-grid boxes (i.e. $k \leq kmt(i+1, j-1), kmt(i+1, j), kmt(i+1, j+1)$), from which the overflow flows out of and into the sidewall. While we are considering the src, the same ideas hold for ent and prd, though for prd (u, v) is directed out of the sidewall.

Let the source transport be M_s, as in Eq. 3, where the regional averages for interior, source and entrainment have been evaluated (see Table 1), and hence M_s. We apply M_s to the three sidewalls to evaluate the corresponding total velocity by ensuring transport

conservation. The three raised overflow boxes have four U-grid corners at $(i, j-2, k), (i, j-1, k), (i, j, k), (i, j+1, k)$ in U-grid coordinates (see Fig. 2). We assume the end points $(i, j-2, k)$ and $(i, j+1, k)$ have no velocity change from zero. For the two interior points at $(i, j-1, k)$ and (i, j, k) in U-grid coordinates we impose:

$$\begin{aligned} u_{(i,j-1,k)} &= -M_s/(2A_{(i,j-1,k)}) \\ u_{(i,j,k)} &= -M_s/(2A_{(i,j,k)}) \end{aligned} \tag{28}$$

where $A_{(i,j,k)}$ is the cross sectional area of the sidewall at the U-grid (i, j, k) position, so from Fig. 2 $A_{(i,j,k)} = dy_{(i,j)}dz_k$ (this should be the same sidewall area used in the tracer advection schemes.) The minus sign reflects that the source flow is into the topography in the decreasing x direction. (Note that the $u_{(i,j,k)}$ here is formally identical to the u_{ovf} used in Section 2B). Hence, the total transport into the sidewall is:

$$u_{(i,j-1,k)}A_{(i,j-1,k)} + u_{(i,j,k)}A_{(i,j,k)} = -M_s \tag{29}$$

as it should be.

This same procedure is followed for ent and prd, with adjustments made in the sign of $u_{(i,j,k)}$ as required by the orientation of the overflow, and consistent with the convention that src,ent flow INTO the sidewall while prd flows OUT (see Fig. 3). We make no limitations on direction: overflows can be "east-west" or "north-south" along grid lines, and can include three or more sidewall T-grid boxes at the same level k. There is no restriction on having "tall" sidewall, i.e. overflows are not restricted to the top of the topography. We assume a uniform overflow velocity along the sidewall as above apart from any changes in area $A_{(i,j,k)}$ along the sidewall, dividing the overflow equally- therefore, the $2s$ in Eq. 28. In general, if there are N adjacent T-grid boxes, then the interior velocities are divided by $(N-1)$ to ensure mass conservation. We apply volume transports M_e and M_p to entrainment and product sidewalls respectively such that by Eq. 16 total water volume is conserved. Using Eq. 17's calculation of product tracers in the advection scheme along the overflow sidewalls ensures tracer conservation.

POP has mulitple options for tracer advection. The precise modification of the sidewall tracer advection formulas depends on the advection scheme. The present POP2 advection schemes that have been modified to account for overflows are the standard 2nd-order centered scheme, and the 3rd-order upwind scheme. For the 2nd-order centered scheme, we refer to the POP2 manual (Smith et al. 2010) for only an x-directed advection, so that the advection operator is:

$$L_T(\varphi) = \frac{1}{\Delta_y}\delta_x(\overline{\Delta_y u_x}^y \bar{\varphi}^x). \tag{30}$$

The terms $\overline{\Delta_y u_x}^y$ are mass fluxes located on the lateral faces of T-grid cells, as well as the tracer $\bar{\varphi}^x$. When one of these faces is a sidewall with an active overflow, then $\overline{\Delta_y u_x}^y$ is replaced by a fraction of the overflow transport (depending on the number of adjacent overflow active points) as in Eqs 3,15,16, and $\bar{\phi}^x$ becomes the overflow tracer (as in Eq 17).

For the 3rd-order upwind advection, continuing to use the notation of the POP2 manual (Smith et al. 2010), and for an east-west oriented src sidewall (as in Fig. 2), the finite-difference expression for the advection of tracers is:

$$ADV(i,j,k) = \frac{-(u_E T^*_E - u_W T^*_W)}{DXT}. \tag{31}$$

where u_E, u_W are T-grid cell face centered velocity components, and T_E, T_W are the east/west cell face centered tracer concentrations determined by a three point interpolation formula. Normally along a sidewall to the west, the velocity $u_W = 0$ as a standard boundary condition. For an OVP sidewall, $u_W \neq 0$, and is the weighted average of the cell face edge velocities (see Fig. 2). Following Eq. 17, we simply set $T^*_W = T_s$ to be the overflow tracer (in this case temperature). For the ent and prd sidewalls a similar procedure is done using T_e and T_p (and all other advected tracers) so that tracer conservation is satisfied.

3B. For Baroclinic/Barotropic Solutions

Allowing non-zero overflow sidewall velocity at depth below the normal kmt topography requires modification of the baroclinic/barotropic velocity solutions as discussed in Section 2B. By definition, the barotropic velocity $U_{(i,j)}$ is the vertical integral of the total velocity $u_{(i,j)}$ from surface to the bottom topography:

$$U_{(i,j)} = \frac{1}{H_{(i,j)}} \int_{-H_{(i,j)}}^{\eta_{(i,j)}} u_{(i,j)} dz \tag{32}$$

where $-H_{(i,j)}$ is the depth of the base of the level $k = kmt(i,j)$. Let us assume for generality that there are one or more sidewall levels above an overflow sidewall. Since by definition $U_{(i,j)}$ must extend down to and include the overflow sidewall, and because by assumption at the overflow level $k = kovf$ the total velocity equals the overflow velocity, we have:

$$\begin{aligned} u_{(i,j,k)} = \ u_{ovf}, \ u'_{(i,j,k)} = u_{ovf} - U_{(i,j)} \qquad & at \quad k = kovf \\ u_{(i,j,k)} = 0, \ u'_{(i,j,k)} = \ -U_{(i,j)} \qquad & at \quad kmt(i,j) < k < kovf \end{aligned} \tag{33}$$

where for clarity we have written the (i,j,k) velocity of Eq. 28 as u_{ovf}. The velocity solution in POP2 is to first solve the baroclinic equations to produce an unnormalized baroclinic velocity u'^*, i.e.

$$\int_{-H_{(i,j)}}^{\eta_{(i,j)}} u'^*_{(i,j,k)} dz \neq 0 \tag{34}$$

which is normalized so

$$\int_{-H_{(i,j)}}^{\eta_{(i,j)}} u'_{(i,j,k)} dz = 0 \tag{35}$$

is satisfied before the barotropic equations are solved. For any overflow columns, i.e. those in which an overflow adjustment to u occurs along a sidewall, we save the $(u'^*_{(i,j,k)}, v'^*_{(i,j,k)})$ unnormalized velocities of all levels k.

We next compute the overflow transports following the presentation in Section 2A. From the overflow transports, the sidewall velocities are evaluated as in Eq. 28. From the

overflow product temperature and salinity we compute a product density, and hence the product injection level, as follows. Let $(\rho_m,\ m = 1, M_{ovf})$ be the set of ambient model densities along the product path for M_{ovf} possible product injection levels (see Table 4 and Table E1). Then the level of product injection is the deepest for which $\rho_p > \rho_m$ but $\rho_p < \rho_{m+1}$, for which the injection level is that associated with $m+1$. We finally compute the forcing term F_{ovf} for the column above the topography needed for the barotropic solution, given by:

$$F_{ovf} = (-M_s,\ -M_e,\ +M_p)/A_{(i,j)} \tag{36}$$

where $A_{(i,j)}$ is the horizontal area of the (i,j) T-grid column above the topography adjacent to an overflow sidewall, and where there are three terms for the source, entrainment and product flows at their respective locations. (Note that in the code Eq. 24 is multiplied by a negative sign; thus we have included the signs as shown in Eq. 36). Then the barotropic equations are solved including these extrae forcing terms resulting in $(U_{(i,j)}, V_{(i,j)})$. Finally, we normalize the baroclinic velocities in an overflow column as follows. We ensure:

$$\begin{aligned} \frac{1}{H_{(i,j)} + \Delta z_a + \Delta z_o} \int_{-H_{(i,j)}-\Delta z_a+\Delta z_o}^{\eta_{(i,j)}} u'_{(i,j,k)} dz = 0 \\ \frac{1}{H_{(i,j)} + \Delta z_a + \Delta z_o} \int_{-H_{(i,j)}-\Delta z_a+\Delta z_o}^{\eta_{(i,j)}} v'_{(i,j,k)} dz = 0 \end{aligned} \tag{37}$$

by including the sidewall contributions as noted above and in Section 3B, Eq. 26. Note that both (u, v) need to be nomalized for the overflow columns.

We allow all overflow product columns to have adjustments done (whereas Fig. 3 only shows one). This was done to avoid issues with a moving product during model execution. This means that adjustments to depth $H_{(i,j)}$ for overflow columns are done for every column every model time step. Note also that the values of the $\vec{u}'^*$ must be saved for all overflow columns, since all are active.

4. Implementation into POP2

Implementation of OFP into POP2 follows the discretization sections 3A and 3B. Here we also add the necessary considerations of bottom topography modifications, associated int, src and ent regions, and selection of prd path and depth. In Appendices D, E and F, we present overviews of the OFP code, input file and restart file for the POP2 implementation respectively.

4A. Bottom Topography Modifications

Bottom topography changes were necessary for implementation of the overflow parameterization into POP2. There were three rationale's for these changes: (1) in some cases changes were necessary to ensure three or more sidewall grid points at the same level so overflows can be permitted; (2) topographic structure in the vicinity of source and/or entrainment contained isolated bowls or less than two grid-point channels inhibiting resolved flow, and (3) some deep downstream choke points were widened to allow deep overflow product more resolved access to certain deep basins.

For the Denmark Strait, the region in the vicinity of the source was altered to reduce the deep fall-off east of the source, and west of the source some isolated bowl grid points were filled in. For the Faroe Bank Channel (FBC), the entire region from the Iceland-Scotland ridge to the actual geographic FBC was widened and flattened, and a small rise was placed on its southerly edge to ensure resolved flow would proceed in the direction of the actual geographic FBC. Some widening of a few regions in the deep product area was done also. A few grid points in the Charlie Gibbs Fracture Zone were deepened and widened, and also the Vema Channel in the central Atlantic. For the Weddell Sea, the shelf was flattened and smoothed somewhat, and the rise for the source overflow was altered as required by the parameterization. Similar changes to the source region shelf was done for the Ross Sea. In addition, the downstream Eltanin Fracture Zone in the south central Pacific was made slightly wider and deeper.

4B. Interior, Source and Entrainment Regions

The starting point are ocean bottom topography maps, as shown in Figs. 4-6. Fig. 4a shows the Greenland-Iceland-Scotland (GIS) Ridge ocean topography to 2000 m, while Fig. 4b shows the same to 4000 m. Each figure shows both the POP2 gx1 resolution (nominally $1^\circ \times 1^\circ$) as well as a high resolution map ($5' \times 5'$). It is apparant that the GIS Ridge obstructs deep water exchange between the Nordic Seas to the north and the subpolar Atlantic Ocean to the south. Two channels allow exchange via overflow processes: the Denmark Strait at 66°N, 27°W, and the Faroe Bank Channel at 62°N, 9°W. The former is approximately 500 m deep, while the latter is between 800 and 900 m. We note that the latter has a complex topography for its channel southeast to southwest of Faroe Island, which we shall comment on shortly.

For the Denmark Strait, we note that cold dense waters just north of the Strait around 67°N, 25°W can overflow through the Strait to an entrainment region around 64°N, 29°W, and hence flow southwestward along the continental slope south of Greenland while descending below 2000 m (see Fig. 4b). For the Faroe Bank Channel, we note that cold dense waters around 62°N, 3°W will fill the channel all the way to the narrowest portion at 62°N, 9°W, which then will overflow through the channel, entrain around 62°N, 11°W and subsequently flow along the continental slope south of Iceland and westward along the southern flank of the Reykjanes Ridge while descending below 2000 m (see Fig. 4b).

Table 3. Longitudes, latitudes and levels for overflow regions. Longitudes in degrees east. Longitude and latitude as pairs for North West, North East, South West and South East points in that order. Int=Interior, Src=Source and Ent=Entrainment Regions. For example, the Ross Sea source region SE point has longitude 184.44E and latitude 77.62°S. Note that two source regions for Faroe Bank Channel are included, SrcW the western and SrcE the eastern. Vertical level and T-grid base depths are given; see Table C1.

Denmark Strait						
Int region:	327.68 65.30	331.68 65.57	328.42 62.57	332.82 62.84	33	504 m
Src region:	334.11 67.94	340.88 68.96	334.76 67.14	341.92 68.18	33	504 m
Ent region:	329.28 65.39	331.68 65.57	329.83 63.83	332.37 64.00	39	928 m
Faroe Bank Channel						
Int region:	342.19 62.51	346.62 63.07	343.14 60.54	347.80 61.08	38	830 m
SrcW region:	351.97 60.76	353.85 61.01	352.40 59.95	354.31 60.20	38	830 m
SrcE region:	355.18 63.46	357.83 63.90	356.92 61.00	359.75 61.43	38	830 m
Ent region:	345.32 62.04	348.02 62.39	345.94 60.85	348.73 61.19	40	1041 m
Ross Sea						
Int region:	182.19 -74.41	184.44 -74.41	182.19 -75.48	184.44 -75.48	34	552 m
Src region:	179.94 -76.55	184.44 -76.55	179.94 -77.62	184.44 -77.62	34	552 m
Ent region:	177.69 -70.67	179.94 -70.67	177.69 -72.81	179.94 -72.81	40	1041 m
Weddell Sea						
Int region:	325.06 -72.81	328.44 -72.81	325.06 -74.41	328.44 -74.41	36	671 m
Src region:	325.06 -75.48	328.44 -75.48	325.06 -76.55	328.44 -76.55	36	671 m
Ent region:	320.56 -72.81	322.81 -72.81	320.56 -73.88	322.81 -73.88	40	1041 m

Fig. 5a shows the Ross Sea topography down to 1000 m, and Fig. 5b the same down to 4000 m. As with Figs. 6a,6b for the Weddell Sea, the Antarctic overflows are characterized by shelves which drop rapidly to very deep basins surrounding the continent. The shelves generally descend towards the continental slope edge, but in a few important cases there are relatively shallow basins separated from the slope edge by sills or small rises. These basins are thus source regions for overflows, similar to the Nordic Sea overflows, though the depth of the source basin is rather shallow. One would expect overflow over the sills and

down the contnental shelf to the shelf-slope break where entrainment occurs, and hence down the slope to the deep basins.

Thus, for the Ross Sea in Figs. 5a,5b we have a source region around 179°W and 77°S with sill at 177°W and 75°S. Such an overflow will proceed down the continenal shelf, turning left (Coriolis turning direction in southern hemisphere) and around the rise at 177°W and 72°S to entrain around 174°-179°W and 71°S before descending further north. For the Weddell Sea we see a source basin at 38°W and 77°S with sill around 31°W and 75°S, an entrainment region around 38°W and 74°S before descent further north.

Thus, we choose the regions as shown in Table 3 for interior, source and entrainment.

Figs. 7a-c show the Nordic Seas regions from Table 3, both as boxed regions and with specific levels. Also shown are product locations from Table 4, as in the following. Figs. 7d-f show the Antarctic overflow regions from Table 3.

4C. Product Path and Depth

Table 4 shows the product path for each overflow. The coordinates are mean values over several points as discussed in Section 3B. The specific path is constrained somewhat by the resolution of the model and requirements of the overflow implementation in POP2. In particular we note that the descent of the overflows is more directly to the deeper basins rather than along the continental slope as suggested by Price and Baringer (1994). Again, this is necessary because of difficulties implementing product injection along the continental slope.

See the end of section 2A for a description of how the product depth is chosen (i.e. the precise level number of Table 4) during a POP2 integration.

Table 4. Longitude, latitude and depth for product injection for four overflows. Longitude in degrees east, latitude degrees north and depth in meters. Longitudes and latitudes mean of several points. Depth is base of vertical grid box (see Table C1).

Overflow and Number	Longitude Latitude	Depth (m)
Denmark Strait		
1	331.73 63.36	1483
2	330.87 63.30	1863
3	329.93 63.44	2075
4	329.24 62.81	2298
5	328.26 63.15	2530
6	327.44 62.91	2768
7	325.12 60.32	3011
Faroe Bank Channel		
1	346.66 61.36	1483
2	345.53 61.65	1863
3	344.81 61.14	2298
4	343.05 60.74	2530
5	340.48 59.88	2768
6	338.03 58.27	3011
Ross Sea		
1	178.81 -72.27	1483
2	178.81 -71.74	1863
3	178.81 -71.21	2075
4	178.81 -70.67	2298
5	178.81 -70.14	2768
6	178.81 -69.60	3256
7	178.81 -69.07	3503
8	183.31 -69.60	3752
9	184.44 -69.60	4001
Weddell Sea		
1	318.31 -73.34	1318
2	317.19 -72.81	1483
3	316.06 -72.27	1863
4	314.94 -71.74	2298
5	314.94 -71.21	2768
6	314.94 -70.67	3256
7	314.94 -70.14	3752
8	314.94 -68.54	4001
9	317.19 -68.00	4251

5. Summary

We have presented the Overflow Parameterization, which is designed for inclusion into the Parallel Ocean Program Version 2 (POP2) ocean component of the Community Climate System Model. This parameterization is a comprehensive parameterization including the effects of source, entrainment and product injection using simple physical models of the flow. A method for baroclinic/barotropic velocity modification was presented that is conservative and stable.

Acknowledgments

We thank the members of the Oceanography Section within the Climate and Global Dynamics division of the National Center for Atmospheric Research (NCAR) for many helpful discussions on various aspects of overflows. We particularly thank Stephen Yeager for assistance with the ETOPO5 data and graphics. We also thank the members of the Gravity Current Entrainment Climate Process Team (CPT) for helpful interactions on various aspects of the overflow parameterization. Adam Phillips of NCAR assisted with graphics. Support for the lead author came from NSF Grant OCE-0336834 for the Climate Process Team on Gravity Current Entrainment. A one year extension of support was made through the Ocean Mixing CPT Proposal 08-407. The computational resources were provided by the Scientific Computing Division of the National Center for Atmospheric Research. NCAR is sponsored by the National Science Foundation.

Appendix A: Derivation of the OFP Equations

Here we present in detail the theory of rotating hydraulic flow through a rectangular channel, from Whitehead et al. (1974), or WLK, and Whitehead (1989). We also present the related theory of the descent, rotation and entrainment of the dense overflow plume after exiting the channel, from Price and Baringer (1994). We use the notation of WLK in this Appendix.

Consider a two-layer rotating homogeneous inviscid fluid in hydrostatic balance, with upper layer density ρ_i and lower layer density ρ_s (the subscripts denoting interior and source respectively). The two-layer fluid occupies two large basins with a connecting raised channel of width W_s between them. It is assumed that steady pumping of fluid from the upstream basin through the channel into the downstream basin occurs, and that the recirculation via an external path occurs in a way that preserves the near stagnant nature of the basins. We thus only need be concerned about the flow of the denser fluid ρ_s through the channel.

A cartesian coordinate system is used with z axis perpendicular to the two basin-connecting channel plane and parallel to the rotation axis. The origin is on one edge of the channel base where it joins the downstream basin. The x axis is perpendicular to the connecting channel and positive away from the channel, while the y axis is parallel to the channel.

Horizontal pressure gradients exist in a two-layer fluid system only if there is a slope in the free surface or in the interface between the fluids. As the free surface slope or interior interface are dependent only on x and y, the horizontal velocity of the denser fluid is depth independent, (i.e. $\bar{u} = \bar{u}(x, y)$). Using ∇ to refer to the horizontal gradient operator, the continuity equation is:

$$\nabla \cdot \bar{u} + \frac{\partial w}{\partial z} = 0 \tag{A1}$$

where $\bar{u}$ is the horizontal vector velocity, $w = dz/dt$ and $d/dt = \partial/\partial t + \bar{u} \cdot \nabla$. Let $h = z_T - z_B$ be the height of the denser fluid ρ_s between the top interface z_T and layer bottom z_B (either channel floor or basin floor). Integrating the continuity equation from z_B to z_T yields:

$$\int_{z_B}^{z_T} \nabla \cdot \bar{u} \; dz + \int_{z_B}^{z_T} \frac{\partial w}{\partial z} dz = 0$$

$$\int_{z_B}^{z_T} \nabla \cdot \bar{u} \; dz = \nabla \cdot \int_{z_B}^{z_T} \bar{u} \; dz - \bar{u} \cdot \nabla (z_T - z_B) = \nabla \cdot \int_{z_B}^{z_T} \bar{u} \; dz - \bar{u} \cdot \nabla h$$

using Leibnitz's rule. The second term is:

$$\int_{z_B}^{z_T} \frac{\partial w}{\partial z} dz = w(z_T) - w(z_B) = dz_T/dt - dz_B/dt = dh/dt$$

Since $\bar{u}$ is depth independent, $\int_{z_B}^{z_T} \bar{u} \; dz = h\bar{u}$, and the vertically integrated continuity equation becomes:

$$\nabla \cdot h\bar{u} - \bar{u} \cdot \nabla h + \frac{\partial h}{\partial t} + \bar{u} \cdot \nabla h = \frac{\partial h}{\partial t} + \nabla \cdot h\bar{u} = 0 \tag{A2}$$

In steady motion, $\frac{\partial h}{\partial t} = 0$, so that

$$\nabla \cdot h\bar{u} = 0 \tag{A3}$$

Defining a streamfunction ψ and noting that $\nabla \cdot \nabla \times (\hat{k}\psi) = 0$, hence $\nabla \times (\hat{k}\psi) = h\bar{u}$ and so $hu = \frac{\partial \psi}{\partial y}$ and $hv = -\frac{\partial \psi}{\partial x}$, where the x and y components of $\bar{u}$ are u and v respectively (i.e. $\bar{u} = (u, v)$).

The steady momentum equations for the denser fluid ρ_s are:

$$\bar{u} \cdot \nabla \bar{u} + f\hat{k} \times \bar{u} + \frac{1}{\rho_s}\nabla p = 0 \tag{A4}$$

where f is the Coriolis parameter and p is the deviation of the pressure from the motionless hydrostatic value. Such a deviation can occur only if the interface between the fluids is sloped, such that at height h in the denser fluid the pressure is $p = (\rho_s - \rho_i)gh$. Thus we write the pressure gradient term as:

$$\frac{1}{\rho_s}\nabla p = \frac{\rho_s - \rho_i}{\rho_0} g \nabla h$$

where $g'_s = \frac{\rho_s - \rho_i}{\rho_0} g$ is referred to as the reduced gravity, and $\rho_0 = 1027$ kg m^{-3} is a reference ocean density. The momentum equations thus become:

$$\bar{u} \cdot \nabla \bar{u} + f\hat{k} \times \bar{u} = -g'_s \nabla h \tag{A5}$$

We form the potential vorticity equation by taking the curl of this equation and using the continuity equation along with the following useful vector identities, where $\bar{A}, \bar{B}, \bar{C}$ are vector fields and χ is a scalar field:

$$\begin{aligned}
\bar{A} \times (\bar{B} \times \bar{C}) &= \bar{B}(\bar{A} \cdot \bar{C}) - \bar{C}(\bar{A} \cdot \bar{B}) \\
\nabla \cdot \chi\bar{A} &= \chi \nabla \cdot \bar{A} + \bar{A} \cdot \nabla\chi \\
\nabla \times (\bar{A} \times \bar{B}) &= \bar{B} \cdot \nabla\bar{A} - \bar{B}\nabla \cdot \bar{A} - \bar{A} \cdot \nabla\bar{B} + \bar{A}\nabla \cdot \bar{B} \\
\nabla \times (\chi\bar{A}) &= \nabla\chi \times \bar{A} + \chi \nabla \times \bar{A} \\
\bar{u} \cdot \nabla\bar{u} &= \nabla(\frac{\bar{u} \cdot \bar{u}}{2}) + \hat{k} \times \bar{u}\zeta \\
\zeta &= \frac{\partial v}{\partial x} - \frac{\partial u}{\partial y}
\end{aligned} \tag{A6}$$

where ζ is the relative vorticity. Using this last identity, we rewrite the momentum equations as:

$$\nabla(\frac{\bar{u} \cdot \bar{u}}{2}) + (\zeta + f)\hat{k} \times \bar{u} = -g'_s \nabla h \tag{A7}$$

Taking the curl of this equation, remembering that the curl of a gradient is zero, we get:

$$\nabla \times \{(\zeta + f)\hat{k} \times \bar{u}\} = \nabla(\zeta + f) \times (\hat{k} \times \bar{u}) + (\zeta + f)\nabla \times (\hat{k} \times \bar{u}) = 0$$

Using the appropriate vector identities from above, this reduces to

$$\hat{k}\{\bar{u} \cdot \nabla(\zeta + f) + (\zeta + f)\nabla \cdot \bar{u}\} = 0$$

Using $\nabla \cdot h\bar{u} = h\nabla \cdot \bar{u} + \bar{u} \cdot \nabla h = 0$ we have

$$\hat{k}\{\bar{u} \cdot \nabla(\zeta + f) - \frac{(\zeta + f)}{h}\bar{u} \cdot \nabla h\} = 0$$

Since

$$\bar{u} \cdot \nabla \frac{(\zeta + f)}{h} h = h\bar{u} \cdot \nabla \frac{(\zeta + f)}{h} + \frac{(\zeta + f)}{h}\bar{u} \cdot \nabla h$$

we have

$$h\bar{u} \cdot \nabla \frac{(\zeta + f)}{h} = 0 \tag{A8}$$

where we note that the coefficient of the non-zero $\hat{k}$ must be zero to satisfy the above equations. Since $\nabla \frac{(\zeta+f)}{h}$ is thus perpendicular to the flow $\bar{u}$, therefore $\nabla \frac{(\zeta+f)}{h}$ must be a function of the stream function ψ, say $F(\psi)$. Thus the potential vorticity equation reduces to:

$$\frac{(\zeta + f)}{h} = F(\psi) \tag{A9}$$

where we call $F(\psi)$ the vorticity potential. Similarly, we take the dot product of $h\bar{u}$ with the momentum equation to obtain another integral of the motion:

$$h\bar{u} \cdot \{\nabla(\frac{\bar{u} \cdot \bar{u}}{2}) + (\zeta + f)\hat{k} \times \bar{u} = -g_s' \nabla h\}$$

Now $\bar{u} \cdot (\hat{k} \times \bar{u}) = 0$, so the above reduces to

$$\bar{u} \cdot \nabla(\frac{\bar{u} \cdot \bar{u}}{2} + g_s' h) = 0$$

Therefore, we define a second function of the stream function, $G(\psi)$, called the Bernouli potential, where

$$\frac{\bar{u} \cdot \bar{u}}{2} + g_s' h = G(\psi) \tag{A10}$$

Note that

$$\nabla G = \frac{\partial G}{\partial \psi}\frac{\partial \psi}{\partial x}\hat{i} + \frac{\partial G}{\partial \psi}\frac{\partial \psi}{\partial y}\hat{j} = \frac{\partial G}{\partial \psi}(-v\hat{i} + u\hat{j})$$

which is perpendicular to $\bar{u} = u\hat{i} + v\hat{j}$.

Now we assume streamlines of ψ are straight down the channel, so $u = 0$ and the solutions become functions of x only. Thus, the x momentum equation is:

$$-fv + g_s' \frac{\partial h}{\partial x} = 0$$

so the Bernoulli potential becomes

$$\frac{v^2}{2} + g_s' h = G(\psi)$$

and the vorticity potential

$$\frac{\frac{\partial v}{\partial x} + f}{h} = F(\psi)$$

We note that

$$\begin{aligned}\frac{\partial G}{\partial \psi} &= \frac{\partial G}{\partial x}\frac{\partial x}{\partial \psi} + \frac{\partial G}{\partial y}\frac{\partial y}{\partial \psi} \\ &= (\frac{\partial x}{\partial \psi}\frac{\partial}{\partial x} + \frac{\partial y}{\partial \psi}\frac{\partial}{\partial y})(\frac{v^2}{2} + g_s' h) \\ &= \frac{\partial x}{\partial \psi}(v\frac{\partial v}{\partial x} + g_s'\frac{\partial h}{\partial x}) \\ &= -\frac{1}{hv}(v\frac{\partial v}{\partial x} + vf) \\ &= -(\frac{\frac{\partial v}{\partial x} + f}{h}) = -F(\psi)\end{aligned}$$

Therefore, if G is a constant than F must be zero.

The Bernoulli potential $G(\psi)$ can now be found from the upstream condition of very small flow (i.e. $v = 0$), so that $G(\psi) = g_s' h_u$, where h_u is the upstream source height of the denser fluid ρ_s above the channel floor. Hence, $dG(\psi)/d\psi = 0$ which then implies that the vorticity potential $F(\psi) = 0$. This means that $F(\psi) = f/(h_u + H) = 0$ where H is the assumed large depth below the channel floor in the upstream basin.

The flow in the channel and the volume transport into the downstream basin can now be evaluated. From $F(\psi) = 0$ we have

$$\frac{\partial v}{\partial x} = -f$$

or

$$v(x) = -fx + v_0 \tag{A11}$$

with v_0 the velocity at $x = 0$. The x momentum equation yields

$$fv = g_s'\frac{\partial h}{\partial x}$$

or

$$\frac{\partial h}{\partial x} = \frac{f^2}{g_s'}x + \frac{fv_0}{g_s'}$$

which integrates to

$$h(x) = -\frac{f^2}{2g_s'}x^2 + \frac{fv_0}{g_s'}x + h_0 \tag{A12}$$

where h_0 is h at $x = 0$. Thus, in the channel the fluid interface is parabolic with maximum height on the side of the channel such that the cross channel pressure gradient is balanced geostrophically by a down channel directed flow. From the velocity solution we further note that the velocity increases away from the maximum height side of the channel to a maximum where the two-layer interface encounters either the bottom of the channel or the opposite side wall.

Following WLK, there are now two unknowns h_0 and v_0. The Bernoulli potential allows evaluate of a relation between these two unknowns, as

$$\frac{v^2}{2} + g_s' h = g_s' h_u$$

can be evaluated at $h = h_0$ for $x = 0$ for which $v = v_0$ and thus

$$v_0 = \sqrt{2g'_s(h_u - h_0)} \tag{A13}$$

There is however, no other relation available to uniquely constrain the problem further. The matter is settle by evaluating the volume transport through the channel subject to all governing equation and boundary condition contraints, and maximizing it. We consider only the case of interface intersection on the bottom of the channel at $x = -x_b$ (i.e. the wide channel condition appropriate for the open ocean overflows). Let M' be the volume transport. Hence

$$M' = \int_{-x_b}^{0} vhdx = \frac{g'_s}{f}\int_{-x_b}^{0} h\frac{\partial h}{\partial x}dx = \frac{g'_s}{2f}(h_0^2 - h^2(-x_b))$$

For the assumed case of $h(-x_b) = 0$ we have

$$M' = \frac{g'_s}{2f}h_0^2$$

We see from the relation Eq(A13) that h_0 must range from 0 up to h_u for non-zero transport. As with WLK, we can use the empirical hydraulic rule of maximal transport, which means $h_0 = h_u$, $v_0 = 0$, $v = -fx$, $h = -\frac{f^2}{2g'_s}x^2 + h_u$ and

$$M_s = \frac{g'_s}{2f}h_u^2 \tag{A14}$$

Further, from $h(-x_b) = 0$ we can evaluate x_b as

$$x_b = \frac{\sqrt{2g'_s h_u}}{f} \tag{A15}$$

which is $\sqrt{2}$ times an internal Rossby radius of deformation of the flow. We note again that $x_b \leq W_s$ for the maximal flow expression for M_s in Eq(A14) to be valid.

The flow which exits the channel is now specified. It has a parabolic height from h_u along one sidewall to 0 at $-x_b$. The velocity increases linearly from 0 to a maximum at $-x_b$. This flow becomes the overflow plume which descends across the continental shelf to the shelf-slope break, where it entrains and descends to greater ocean depth. To relate this flow to the source for the descent and entrainment, we can take two approaches. Both assume a rectangular geometry for the overflow as it exits the channel, but use different widths for the flow.

We first compute a mean height h_s for the flow as it exits the channel:

$$h_s = \frac{1}{x_b}\int_{-x_b}^{0} h(x)\ dx = \frac{1}{x_b}\int_{-x_b}^{0} (-\frac{f^2x^2}{g'_s} + h_u)\ dx = \frac{2}{3}h_u \tag{A16}$$

making use of Eq(A12). We either assume this flow covers the entire channel width W_s, or we use the flow width x_b. Using x_b allows more dynamic freedom and consistency to the parameterization, but most applications use the fixed channel width W_s, as we will here.

Given the width of the source flow W_s, the speed U_s of the source waters as they exit the channel of rectangular area A_s is then given by

$$\begin{aligned} U_s &= M_s/A_s \\ A_s &= h_s W_s \end{aligned} \tag{A17}$$

The overflow plume is assumed to descend the continental shelf of slope α to the continental shelf-slope break a distance x_{ssb} downstream without mixing ambient water (note that here we use x as a downstream coordinate, while previously we have used it as a cross-stream coordinate; this is because of the different origins of the channel transport and downstream entrainment parameterizations). The descending overflow turns nearly at right angles to the slope α by Coriolis acceleration. Thus overflow acceleration downslope is assumed to be geostrophically balanced by the Coriolis acceleration at the shelf-slope break, where the overflow plume speed is:

$$U_{ssb} = \frac{g'_e \alpha}{f} \tag{A18}$$

where reduced gravity g'_e is defined as:

$$g'_e = \frac{\rho'_s - \rho_e}{\rho_0} g \tag{A19}$$

with ρ'_s the source density ρ_s at the entrainment depth d_e, $\rho_0 = 1027$ kg m^{-3} is a reference ocean density. We assume here a point-model of entrainment, i.e. that it occurs at only one place for the overflow plume at the depth d_e. Thus the average speed during descent is given by:

$$U_{avg} = \frac{1}{2}(U_s + U_{ssb}) \tag{A20}$$

We now assume that bottom drag acts on the flow during descent, causing it to spread laterally compared to its channel-confined width. This spreading is according to an Ekman number K given by the ratio of mean drag to Coriolis acceleration:

$$K = \frac{C_d U_{avg}^2 / \frac{1}{2}(h_s + h_{ssb})}{f U_{avg}} = \frac{C_d U_{avg}}{\frac{1}{2}(h_s + h_{ssb}) f} \tag{A21}$$

where C_d is the bottom drag coefficient and where h_{ssb} is the plume height at the shelf-slope break given by volume conservation:

$$h_{ssb} = \frac{U_s h_s W_s}{U_{ssb} W_{ssb}} \tag{A22}$$

with the flow width specified by:

$$W_{ssb} = W_s + 2K x_{ssb} \tag{A23}$$

This expression derives from a force balance between downslope acceleration, Coriolis acceleration and surface drag. As the flow proceeds downslope it spreads at a rate proportional to distance traveled (ultimately x_{ssb}) and the ratio of the drag to Coriolis acceleration. We

can think of this as an initial downslope motion dragged by bottom friction but mostly turned perpendicular by Coriolis acceleration, the deviation from right angle producing the lateral spreading at a rate just noted.

Eqs A21, A22 and A23 form a quadratic set for the unknown h_{ssb}, which can be solved taking the positive root as follows:

$$\begin{aligned} a &= fW_s \\ b &= fW_s h_s + 4C_d U_{avg} x_{ssb} - M_s f/U_{ssb} \\ c &= -fM_s h_s/U_{ssb} \\ h_{ssb} &= (-b + \sqrt{b^2 - 4ac})/2a \end{aligned} \tag{A24}$$

At the shelf-slope break a distance x_{ssb} downstream from the channel, the overflow plume is assumed to pour over the break and descend downslope. Because of the downslope acceleration and thinning of the plume as it spreads, instabilities can occur at the interface with ambient waters producing entrainment into the plume. This will occur if the plume flow speed U_{ssb} exceeds the gravity wave speed of interfacial waves, $\sqrt{g'_e h_{ssb}}$, determined by a geostrophic Froude number:

$$F_{geo} = \frac{U_{ssb}}{\sqrt{g'_e h_{ssb}}} \tag{A25}$$

If $F_{geo} < 1$ the flow is stable and no mixing occurs, and is termed sub-critical. $F_{geo} = 1$ is critical condition and $F_{geo} > 1$ is termed super-critical, for which the flow is unstable and mixing occurs.

Following Price and Baringer (1994), we assume that such instabilities and subsequent mixing with ambient waters slow the overflow plume, reduce it's density contrast with ambient water, and thicken it in such a manner that the resulting Froude number of the mixed waters is 1 or less, i.e. it is stable. As the subsequent flow descends downslope we assume it maintins stability by maintaining its overall geometry and mixed properties, and thus becomes the final product waters.

We can roughly estimate the amount of mixing with ambient waters necessary to ensure overflow plume stability. Let the mixed water Froude number be given by:

$$F^*_{geo} = \frac{U^*_{ssb}}{\sqrt{g'^*_e h^*_{ssb}}} \tag{A26}$$

where $*$ refers to the final mixed water properties. For mixed water stability (i.e. no further mixing) we require that

$$F^*_{geo} = 1 \tag{A27}$$

We assume the mixing is with stationary ambient water. Let ϑ be the fraction of ambient water entrained compared to the total ($0 \leq \vartheta \leq 1$). We assume U_{ssb} is slowed to

$$U^*_{ssb} = U_{ssb}(1 - \vartheta) \tag{A28}$$

It is reasonable to assume the ambient water mixing does not change the width W_{ssb} of the flow, but only its depth. Thus

$$h^*_{ssb} = h_{ssb} U_{ssb} / U^*_{ssb} \tag{A29}$$

to conserve momentum before and after mixing. Finally, we assume that the change in reduced gravity can be approximated by:

$$g'^*_e = g'_e (1 - \vartheta) \tag{A30}$$

which can be derived from Eq. A19 using $\rho'^* = \rho'_s(1-\vartheta) + \vartheta\rho_e$ and that $\rho_e/\rho'_s \approx 1$. In actuality the dependence of g'^*_e via density is non-linear in ϑ, so this is a rough approximation. Thus we have

$$F^*_{geo} = 1 = \frac{U_{ssb}(1-\vartheta)}{\sqrt{g'_e h_{ssb}}} = F_{geo}(1-\vartheta) \tag{A31}$$

or

$$\vartheta = 1 - \frac{1}{F_{geo}} \tag{A32}$$

Price and Baringer (1994) give an alternate expression for mixing fraction as:

$$\vartheta = 1 - \frac{1}{F^{2/3}_{geo}} \tag{A33}$$

which yields a lower mixing fraction. They give no explanation for this form though. We can argue heuristically for this as follows. The reduced gravity g'_e can be considered as a buoyancy which is transported by the overflow source at speed U_{ssb} with volume flux $h_{ssb} W(x_{ssb}) U_{ssb}$ with the transport flux $g'_e(h_{ssb} W(x_{ssb}) U_{ssb})$. Normalizing this to per unit width $W(x_{ssb})$ of the flow, we have a buoyancy flux at the shelf-slope break:

$$B_{ssb} = g'_e h_{ssb}\ U_{ssb}\ . \tag{A34}$$

But $g'_e h_{ssb}$ is the square of the interfacial wave speed between the source waters at density ρ'_s and the ambient waters ρ_e. Faster interfacial wave speed implies more stable source flow and thus less mixing, as interfacial waves can propagate away disturbances. Since the scaling of the buoyancy flux in Eq A34 is cube of speed, we argue that $(B^{1/3}_{ssb}/U_{ssb})$ gives the fraction of source that is unmixed with the ambient, with a corresponding entrainment fraction:

$$\vartheta = 1 - \frac{B^{1/3}_{ssb}}{U_{ssb}}\ . \tag{A35}$$

Using Eq A34 in A35 results in Eq A33. We use Eq A33 in the OFP.

Given the mixing fraction ϑ, the entrainment volume transport M_e can be evaluated as:

$$M_e = M_s \vartheta / (1 - \vartheta) \tag{A34}$$

and the total product transport as:

$$M_p = M_s + M_e \tag{A35}$$

The product water temperature and salinity (T_p and S_p respectively) are evaluated by:

$$\begin{aligned} T_p &= T_s(1-\vartheta) + T_e\vartheta \\ S_p &= S_s(1-\vartheta) + S_e\vartheta \end{aligned} \tag{A36}$$

and similarly for other tracers if present.

Appendix B: Application of OFP to Observations

In this section we apply the overflow parameterization of Section 2A to four important ocean overflows using observations: two Nordic Sea overflows, Denmark Strait and Faroe Bank Channel, and two Antarctic overflows, Ross Sea and Weddell Sea. Such an application allows us to check the parameterization with observed data and also select parameter values, both of which prove critical for implemention into POP2.

To proceed, we need to compare density profiles of interior and source regions using the region boundaries of Table 3. The basic physics is that such density differences will drive an overflow through the connecting channel (Appendix A). Here we follow Whitehead (1989).

Figs. 8-11 show density profiles for interior and source regions for the Denmark Strait, Faroe Bank Channel, Ross Sea and Weddell Sea overflows respectively. The density profiles are relative to the surface.

In each case, with increasing depth the source region density begins to exceed that of the interior region at some depth, the excess increasing with depth down to the channel floor (or sill depth) and deeper depending on the depth of the source basin.

We use Levitus annual mean temperature and salinity data (Levitus et al. 1998, Steele et al. 2001) interpolated onto the POP2 gx1 horizontal and 60 level vertical grid (see Table C1), and then averaged over the regions of Table 3, to compute these density profiles. Such profiles show very nicely the density differences which drive the overflows. The vertical depth over which the source density exceeds the interior density down to the channel floor or sill depth specifies the value of the upstream source thickness h_u.

Referring to Table 1, there are thus five more parameters to specify, and the interior, source and entrainment depths. The latitude can be approximated from Table 3, and the interior/source/entrainment depths approximately from Figs. 4-6. The remaining four parameters are taken from Price and Baringer (1994). The Ross Sea parameters are set identical to those of the Weddell Sea. The channel widths W_s and distance from strait to shelf-slope break x_{ssb} are compatible with the high resolution topography of Figs. 4-6. The bottom shelf slope α is greatest for the Antarctic overflows, less for Denmark Strait and least for Faroe Bank Channel. We use a slightly lower value of the slope for the Denmark Strait than that of Price and Baringer (1994), but still within the range shown in Legg et.al (2008). The bottom drag coefficient C_d is not known very well at all, so we choose the value of Price and Baringer (1994) and keep it fixed for all four overflows.

With all parameters in Table 1 specified, and with the regional, annual mean temperatures and salinities computed from the Levitus data as just described, we can then evaluate the resulting overflow properties using the overflow parameterization presented in Section 2A. The results are presented in Tables B1-B4.

Table B1. Denmark Strait Overflow Parameters and Transports. The transports are computed with the parameters and regional, annual mean T,S shown using the overflow parameterization of Section 2A. Note that $R_{def} = \sqrt{g'_s\ h_u}/f$.

Symbol	Description	Value
	Input Parameters	
ϕ	latitude of overflow	65°N
h_u	upstream thickness of the source water	450 m
h_s	source thickness at channel	300 m
W_s	width of straight	50 km
x_{ssb}	distance from straight to shelf-slope break	100 km
α	maximum bottom slope near shelf/slope break	.025
C_d	bottom shelf drag coefficient	.003
	Interior	
T_i, S_i	temperature and salinity	(5.305 °C, 35.043 psu)
d_s, ρ_i	depth and density	(483 m, 1029.890 kg m^{-3})
	Source	
T_s, S_s	temperature and salinity	(0.314 °C, 34.914 psu)
d_s, ρ_s	depth and density	(483 m, 1030.302 kg m^{-3})
g'_s	reduced gravity	.0039 m^{2}s^{-1}
R_{def}	Rossby radius of deformation	9.5 km
A_s	cross sectional area	15.0 km^2
U_s	flow speed	.201 ms^{-1}
M_s	transport	3.016 Sv
	Entrainment	
T_e, S_e	temperature and salinity	(4.408 °C, 34.987 psu)
d_e, ρ_e	depth and density	(879 m, 1031.768 kg m^{-3})
ρ'_s	source density at entrainment depth	1032.155 kg m^{-3}
g'_e	reduced gravity	.0037 m^{2}s^{-1}
U_{ssb}	geostrophic flow speed	.699 ms^{-1}
U_{avg}	average flow speed	.450 ms^{-1}
K	Ekman number	.0551
W_{ssb}	spreading width	61.0 km
h_{ssb}	spreading depth	70.7 m
F_{geo}	Froude number	1.37
ϑ	entrainment fraction	0.189
M_e	transport	0.701 Sv
	Product	
T_p, S_p	temperature and salinity	(1.086 °C, 34.928 psu)
ρ_{p3000}	density at z=3000 m	1041.700 kg m^{-3}
M_p	transport	3.717 Sv

Note that we include the Rossby radius of deformation $R_{def} = \sqrt{g'_s\ h_u}/f$, which must be less than channel width W_s (see Appendix A, Eq A15) for the transport formula Eq. 3 to be applicable. We discuss the results in turn. In this discussion, we will refer to the Table of Observations (TO) from Legg et al. (2008). This table has estimates of many overflow properties for reference.

Table B1 shows the Denmark Strait overflow results. The source transport of 3.0 Sv agrees well with the TO value of 2.9 Sv, and estimates from Dye et al. (2007) of 3-4 Sv, and Macrander et al. (2007) of 2.5-3.7 Sv.

The entrainment transport, and therefore the product, is another matter. For this overflow and the Faroe Bank Channel as well, the entrainment is much smaller than given in the TO. For the Denmark Strait, the TO gives 2.3 Sv while our Table B1 gives only 0.7 Sv. The mixing parameter ϑ (i.e. the ratio of entrainment to total product transport) is about 0.44 for TO compared to 0.19 from Table B1.

We note that in our case the entrainment is that for the overflow parameterization, while when implemented into POP2 the actual entrainment would include explicitly computed transport. It is not possible to completely separate the two, but we note that our entrainment is less than those estimated in TO as it should be.

The product water temperature is thus weighted towards the source, and therefore is cold compared with TO (1.1 °C as against 2.1 °C respectively). The salinity comparison is less clear, with the present overflow data yielding somewhat saltier values compared to TO (34.93 psu as against 34.84 respectively). The issue of the entrainment of course has bearing on how deep the product waters will descend, since entrained waters dilute the source and make it less dense. Thus the total product transport is 3.7 Sv, less than that of the TO of 5.2 Sv.

Tables B2a and B2b present results for the Faroe Bank Channel. As mentioned before, the unusual geometry of the Faroe Bank Channel raises the issue of where to place the source region. If one assumes that the dense Nordic Sea waters fills the channel up to its narrowest part, then one could use a region along the Faroe Shetland Channel, which is easier to model. For completeness, we include results for two source regions, one close to the narrowest portion of the channel, and a second eastward somewhat towards the Shetland Islands. The latter uses the overflow parameters from Price and Baringer (1994), while the former uses a larger slope and smaller shelf to slope break distance in keeping with a closer position to the entrainment region. The former also uses a somewhat larger upstream source thickness h_u, in keeping with Fig. 9. Notice also that in addition to the issue of the unusual geometry, the narrowness of the strait is barely larger than the Rossby radius of deformation, a requirement necessary for applicability of the maximal geostrophic transport Eq. 3. Whitehead (1989) showed that for R_{def} of order W_s, actual transport can be up to 20% less than the maximal.

Table B2a. Faroe Bank Channel Overflow Parameters and Transports for the western source. The transports are computed with the parameters and regional, annual mean T,S shown using the overflow parameterization of Section 2A. Note that $R_{def} = \sqrt{g'_s\ h_u}/f$.

Symbol	Description	Value
	Input Parameters	
ϕ	latitude of overflow	62°N
h_u	upstream thickness of the source water	350 m
h_s	source thickness at channel	233 m
W_s	width of straight	15 km
x_{ssb}	distance from straight to shelf-slope break	150 km
α	maximum bottom slope near shelf/slope break	.022
C_d	bottom shelf drag coefficient	.003
	Interior	
T_i, S_i	temperature and salinity	(6.866 °C, 35.166 psu)
d_s, ρ_i	depth and density	(787 m, 1031.137 kg m^{-3})
	Source	
T_s, S_s	temperature and salinity	(2.289 °C, 35.029 psu)
d_s, ρ_s	depth and density	(787 m, 1031.632 kg m^{-3})
g'_s	reduced gravity	.0047 m^{2}s^{-1}
R_{def}	Rossby radius of deformation	10.0 km
A_s	cross sectional area	3.5 km^2
U_s	flow speed	.643 ms^{-1}
M_s	transport	2.251 Sv
	Entrainment	
T_e, S_e	temperature and salinity	(6.021 °C, 35.135 psu)
d_e, ρ_e	depth and density	(985 m, 1032.133 kg m^{-3})
ρ'_s	source density at entrainment depth	1032.544 kg m^{-3}
g'_e	reduced gravity	.0039 m^{2}s^{-1}
U_{ssb}	geostrophic flow speed	.669 ms^{-1}
U_{avg}	average flow speed	.656 ms^{-1}
K	Ekman number	.099
W_{ssb}	spreading width	44.7 km
h_{ssb}	spreading depth	75.2 m
F_{geo}	Froude number	1.23
ϑ	entrainment fraction	0.131
M_e	transport	0.338 Sv
	Product	
T_p, S_p	temperature and salinity	(2.776 °C, 35.043 psu)
ρ_{p3000}	density at z=3000 m	1041.518 kg m^{-3}
M_p	transport	2.589 Sv

Table B2b. Faroe Bank Channel Overflow Parameters and Transports for the eastern source. The transports are computed with the parameters and regional, annual mean T,S shown using the overflow parameterization of Section 2A. Note that $R_{def} = \sqrt{g'_s\ h_u}/f$.

Symbol	Description	Value
	Input Parameters	
ϕ	latitude of overflow	62°N
h_u	upstream thickness of the source water	300 m
h_s	source thickness at channel	200 m
W_s	width of straight	15 km
x_{ssb}	distance from straight to shelf-slope break	250 km
α	maximum bottom slope near shelf/slope break	.015
C_d	bottom shelf drag coefficient	.003
	Interior	
T_i, S_i	temperature and salinity	(6.866 °C, 35.166 psu)
d_s, ρ_i	depth and density	(787 m, 1031.137 kg m^{-3})
	Source	
T_s, S_s	temperature and salinity	(-0.655 °C, 34.896 psu)
d_s, ρ_s	depth and density	(787 m, 1031.785 kg m^{-3})
g'_s	reduced gravity	.0062 m^{2}s^{-1}
R_{def}	Rossby radius of deformation	10.6 km
A_s	cross sectional area	3.0 km^2
U_s	flow speed	.721 ms^{-1}
M_s	transport	2.163 Sv
	Entrainment	
T_e, S_e	temperature and salinity	(6.021 °C, 35.135 psu)
d_e, ρ_e	depth and density	(985 m, 1032.133 kg m^{-3})
ρ'_s	source density at entrainment depth	1032.713 kg m^{-3}
g'_e	reduced gravity	.0055 m^{2}s^{-1}
U_{ssb}	geostrophic flow speed	.645 ms^{-1}
U_{avg}	average flow speed	.683 ms^{-1}
K	Ekman number	.132
W_{ssb}	spreading width	80.9 km
h_{ssb}	spreading depth	41.5 m
F_{geo}	Froude number	1.35
ϑ	entrainment fraction	0.180
M_e	transport	0.474 Sv
	Product	
T_p, S_p	temperature and salinity	(0.545 °C, 34.939 psu)
ρ_{p3000}	density at z=3000 m	1041.789 kg m^{-3}
M_p	transport	2.637 Sv

The resulting overflow transports are very similar. Both source regions produce transports around 2.2 to 2.3 Sv, comparable to the TO of 1.9 Sv. These source transports are consistent with the estimates from current meter measurements of Dye et al. (2007) of 2.1 ±0.2 Sv. Again, the entrainment is much smaller than that implied in the TO, with Tables B2a and B2b yielding .34 and .47 Sv respectively compared to 1.5 Sv from TO. The product water properties differ between the two though, with the eastern source colder and fresher than the western, resulting in an eastern source density larger than the western. For the POP2 implementation, we chose the eastern (Table B2b) source region for the Faroe Bank Channel overflow.

Table B3 presents the results for the Ross Sea overflow. The source transport is 0.77 Sv, somewhat higher than the TO 0.6 Sv. The entrainment is more robust compared to the Nordic Overflows, with 0.52 Sv entrainment and ϑ=0.40 . The total product is thus 1.28 Sv compared with the TO of 2 Sv. The entrainment is stronger because the slope α is larger and because the entrainment waters are less dense relative to their source than their Nordic conterparts, resulting in an entrainment reduced gravity g'_e which is larger than the source reduced gravity g'_s.

Table B4 presents the results for the Weddell Sea overflow. The source transport in this case is very small, at only 0.17 Sv, compared to the TO value of 1 Sv. The entrainment is relatively robust as in the Ross Sea case, resulting in a product transport of 0.28 Sv. The TO value is 5 Sv. From Fig. 11 we see that the density difference between interior and source is the main cause of this anemic overflow, compared with the Ross Sea. We thus cannot account for the large Weddell Sea product transport in TO.

Tables B1-B4 show overflow transports based on annual mean observed temperature and salinity. We computed the monthly equivalents of Tables B1-B4 (not shown) from the observed data (Levitus et al. 1998, Steele et al. 2001). All four overflows have seasonal variation, but annual means of the monthly transports are within 0.05 Sv of those in Tables B1-B4. For the Denmark Strait overflow, there is a semi-annual cycle with maxima in February and July, with minima in April and August, and with product transport ranging from 3.13 to 4.31 Sv, or about ±15 % of the mean. For the Faroe Bank Channel overflow, we find an annual cycle with peak in January and minimum in June, with a product transport range from 2.51 to 2.89 Sv, or about ±7 % of the mean. For the Ross Sea overflow there is an annual cycle with peak in local summer (December) and minimum in local fall (April), with product transport ranging from 0.97 to 1.67 Sv, or about ±27 % of the mean. For the Weddell Sea overflow, we find another semi-annual cycle with local maxima in January and August, minima in April and October, with a product transport ranging from .20 Sv (October) to 0.47 Sv (January), or -30% to +70% of the mean.

These results indicate a noticeable seasonal cycle in the estimated overflow transport, with the Nordic overflows peaking in local winter while the Antarctic overflows peak in local summer.

Table B3. Ross Sea Overflow Parameters and Transports. The transports are computed with the parameters and regional, annual mean T,S shown using the overflow parameterization of Section 2A. Note that $R_{def} = \sqrt{g'_s\ h_u}/f$.

Symbol	Description	Value
	Input Parameters	
ϕ	latitude of overflow	75°S
h_u	upstream thickness of the source water	400 m
h_s	source thickness at channel	267 m
W_s	width of straight	100 km
x_{ssb}	distance from straight to shelf-slope break	150 km
α	maximum bottom slope near shelf/slope break	.032
C_d	bottom shelf drag coefficient	.003
	Interior	
T_i, S_i	temperature and salinity	(0.348 °C, 34.713 psu)
d_s, ρ_i	depth and density	(528 m, 1030.350 kg m^{-3})
	Source	
T_s, S_s	temperature and salinity	(-1.508 °C, 34.747 psu)
d_s, ρ_s	depth and density	(528 m, 1030.492 kg m^{-3})
g'_s	reduced gravity	.0014 m^{2}s^{-1}
R_{def}	Rossby radius of deformation	5.3 km
A_s	cross sectional area	26.7 km^2
U_s	flow speed	.0289 ms^{-1}
M_s	transport	0.770 Sv
	Entrainment	
T_e, S_e	temperature and salinity	(0.599 °C, 34.731 psu)
d_e, ρ_e	depth and density	(985 m, 1032.478 kg m^{-3})
ρ'_s	source density at entrainment depth	1032.653 kg m^{-3}
g'_e	reduced gravity	.0017 m^{2}s^{-1}
U_{ssb}	geostrophic flow speed	.381 ms^{-1}
U_{avg}	average flow speed	.205 ms^{-1}
K	Ekman number	.031
W_{ssb}	spreading width	109.2 km
h_{ssb}	spreading depth	18.5 m
F_{geo}	Froude number	2.16
ϑ	entrainment fraction	0.402
M_e	transport	0.517 Sv
	Product	
T_p, S_p	temperature and salinity	(-0.661 °C, 34.741 psu)
ρ_{p3000}	density at z=3000 m	1041.804 kg m^{-3}
M_p	transport	1.287 Sv

Table B4. Weddell Sea Overflow Parameters and Transports. The transports are computed with the parameters and regional, annual mean T,S shown using the overflow parameterization of Section 2A. Note that $R_{def} = \sqrt{g'_s\ h_u}/f$.

Symbol	Description	Value
	Input Parameters	
ϕ	latitude of overflow	75°S
h_u	upstream thickness of the source water	300 m
h_s	source thickness at channel	200 m
W_s	width of straight	100 km
x_{ssb}	distance from straight to shelf-slope break	150 km
α	maximum bottom slope near shelf/slope break	.032
C_d	bottom shelf drag coefficient	.003
	Interior	
T_i, S_i	temperature and salinity	(0.096 °C, 34.667 psu)
d_s, ρ_i	depth and density	(528 m, 1030.331 kg m^{-3})
	Source	
T_s, S_s	temperature and salinity	(-0.677 °C, 34.673 psu)
d_s, ρ_s	depth and density	(528 m, 1030.387 kg m^{-3})
g'_s	reduced gravity	.0005 m^{2}s^{-1}
R_{def}	Rossby radius of deformation	2.8 km
A_s	cross sectional area	20.0 km^2
U_s	flow speed	.0085 ms^{-1}
M_s	transport	0.170 Sv
	Entrainment	
T_e, S_e	temperature and salinity	(0.379 °C, 34.677 psu)
d_e, ρ_e	depth and density	(985 m, 1032.454 kg m^{-3})
ρ'_s	source density at entrainment depth	1032.536 kg m^{-3}
g'_e	reduced gravity	.0008 m^{2}s^{-1}
U_{ssb}	geostrophic flow speed	.179 ms^{-1}
U_{avg}	average flow speed	.094 ms^{-1}
K	Ekman number	.019
W_{ssb}	spreading width	105.7 km
h_{ssb}	spreading depth	9.0 m
F_{geo}	Froude number	2.13
ϑ	entrainment fraction	0.395
M_e	transport	0.110 Sv
	Product	
T_p, S_p	temperature and salinity	(-0.260 °C, 34.675 psu)
ρ_{p3000}	density at z=3000 m	1041.698 kg m^{-3}
M_p	transport	0.280 Sv

Inspecting the observed ρ_{3000} density profiles in Table B5 for the product path and comparing with the overflow product density (at same level) shown in Tables B1-B4 shows that such product waters should descend to the lowest levels except for the Weddell Sea, which should descend to the 3256 m level only.

Using the monthly observed data (not shown), we can estimate the seasonal ranges of the density at z=3000 m. For Denmark Strait, the range is from 1041.650 (December) to 1041.755 (March) kg m^{-3} or a .105 kg m^{-3} range. For Faroe Bank Channel, the range is from 1041.731 (January) to 1041.841 (September) kg m^{-3} or a .110 kg m^{-3} range. For Ross Sea, the range is from 1041.785 (March) to 1041.855 (November) kg m^{-3} or a .07 kg m^{-3} range. For the Weddell Sea, the range is from 1041.678 (December) to 1041.725 (January) kg m^{-3}, or a .047 kg m^{-3} range. Usually the greatest density occurs when the entrainment parameter ϑ is the smallest, as one might expect. These seasonal ranges in product density are not large enough to change the level of product injection for the Nordic Sea and Ross Sea overflows, but would dramatically change the injection depth for the Weddell Sea overflow (see Table B5). For that overflow, seasonal variation in product depth would range from 1483 to 4001 m.

In summary, we consider these overflow calculations based on observational input and parameter values from Price and Baringer (1994) to agree reasonably well with observed and estimated transports. The issue of how to compare entrainment and product estimates between the parameterization and observations remains however. The parameter values chosen to yield near-observed transports for near-observed inputs gives confidence that when implemented into POP2 or any other z-coordinate ocean model, the resulting overflow impacts should be fairly realistic. Note again that for the POP2 implementation we chose the eastern (Table B2b) source region for the Faroe Bank Channel overflow.

Table B5. Depth and density of product injection for four overflows (see Table 4 for geographic locations). Depth in meters. Depth is that of the base of the vertical grid box (see Table C1).

Overflow and Number	Depth (m)	ρ_{3000} kg m^{-3}
Denmark Strait		
1	1483	1041.287
2	1863	1041.329
3	2075	1041.388
4	2298	1041.394
5	2530	1041.423
6	2768	1041.510
7	3011	1041.563
Faroe Bank Channel		
1	1483	1041.294
2	1863	1041.327
3	2298	1041.422
4	2530	1041.481
5	2768	1041.482
6	3011	1041.513
Ross Sea		
1	1483	1041.649
2	1863	1041.658
3	2075	1041.691
4	2298	1041.673
5	2768	1041.685
6	3256	1041.695
7	3503	1041.695
8	3752	1041.692
9	4001	1041.698
Weddell Sea		
1	1318	1041.671
2	1483	1041.680
3	1863	1041.687
4	2298	1041.697
5	2768	1041.714
6	3256	1041.720
7	3752	1041.724
8	4001	1041.728
9	4251	1041.738

Appendix C: POP2 Vertical Grid

Here we present the POP2 60 level vertical grid for reference, as shown below in Table C1. The vertical layers are tracer layers, with temperature T and salinity S given for mid-layer depths (i.e. T-grid levels).

Table C1. Vertical Levels in POP2, in meters. Level number in left column; layer top, mid and bottom depths rounded to the nearest meter.

Level	Top Depth	Mid-level Depth	Bottom Depth
1	0	5	10
2	10	15	20
3	20	25	30
4	30	35	40
5	40	45	50
6	50	55	60
7	60	65	70
8	70	75	80
9	80	85	90
10	90	95	100
11	100	105	110
12	110	115	120
13	120	125	130
14	130	135	140
15	140	145	150
16	150	155	160
17	160	165	170
18	170	175	181
19	181	186	192
20	192	198	203
21	203	210	216
22	216	223	229
23	229	236	244
24	244	251	259
25	259	268	276
26	276	285	295
27	295	305	315
28	315	327	338

Table C1. Continued. Vertical Levels in POP2, in meters. Level number in left column; layer top, mid and bottom depths rounded to the nearest meter.

Level	Top Depth	Mid-level Depth	Bottom Depth
29	338	351	364
30	364	378	393
31	393	409	425
32	425	443	462
33	462	483	504
34	504	528	552
35	552	579	607
36	607	639	671
37	671	708	744
38	744	787	830
39	830	879	928
40	928	985	1041
41	1041	1106	1171
42	1171	1245	1318
43	1318	1400	1483
44	1483	1574	1665
45	1665	1764	1863
46	1863	1969	2075
47	2075	2186	2298
48	2298	2414	2530
49	2530	2649	2768
50	2768	2889	3011
51	3011	3133	3256
52	3256	3380	3503
53	3503	3628	3752
54	3752	3876	4001
55	4001	4126	4251
56	4251	4375	4500
57	4500	4625	4750
58	4750	4875	5000
59	5000	5125	5250
60	5250	5375	5500

Appendix D: POP2 OFP Code

We present in this appendix a very brief discussion of certain aspects of the overflow code in POP2. In particular, Table E1 relates the overflow parameters of Table 1 in this technical report to the input parameter names and those used in the overflow transport routine. Also, we provide a brief description in Table E2 of the routines in the overflow module in POP2. These are mostly presented in order of their call, from initialization through advection, transport, and final velocity solution for the overflow columns. It is hoped that such a brief overview will aid the user in implementing the overflow code into other ocean climate models.

Table D1. Relation between Technical Note overflow parameters with POP2 Overflow Code variable names. First column is the symbol used in this document (see Table 1); the second column gives the parameter name upon input to POP2, and the third column gives the variable name used in the subroutine ovf-transports (see Table E2). Note that a Fortran 90 derived type of ovf(n)%ovf-params is used to store the input parameters, where n is the index of the nth overflow. (Also note that the dashes in these expressions are underscores in the code.)

Symbol	Input name	As used in ovf-transports
ϕ	ovf(n)%ovf-params%lat	lat
W_s	ovf(n)%ovf-params%width	Ws
h_u	ovf(n)%ovf-params%source-thick	hu
x_{ssb}	ovf(n)%ovf-params%distnc-str-ssb	xse
α	ovf(n)%ovf-params%bottom-slope	alpha
C_d	ovf(n)%ovf-params%bottom-drag	cd

Table D2. List of overflow routines in POP2 and description. The POP2 module (other than the overflow module) which calls the overflow routine is listed in parantheses. "init" is a four-letter designator for initialization of the overflow code. "ovf" is a three-letter designator of overflow routines. "kmt" is the POP bottom topography index array. "HU" is the vertical depth from surface to bottom topography, or to the overflow sidewall. (Note that the dashes in these expressions are underscores in the code.)

Routine	Description
init-overflows1	reads overflow input (initial.F90)
init-overflows2	distributes kmt; computes mask (initial.F90)
init-overflows-kmt	modifies kmt if desired
init-overflows-mask	computes mask for overflow regions
init-overflows3	calls ovf-solvers-9pt to set stencil weights (initial.F90)
init-overflows4	makes overflow diagnostic file (initial.F90)
init-overflows5	computes regional tracer values (initial.F90)
ovf-write-restart	writes overflow restart file (step-mod.F90)
ovf-read-restart	reads overflow restart file (init-overflows1)
ovf-read-broadcast	broadcasts overflow restart data to all processors
ovf-diag	for overflow diagnostics (baroclinic.F90)
ovf-advt	sets overflow sidewall advective transports (advection.F90)
ovf-wtkb-check	diagnostic routine to print w at bottom of column (advection.F90)
ovf-UV-check	diagnostic routine to print out overflow U,V velocities
ovf-Utlda	saves unnormalized baroclinic column velocities (baroclinic.F90)
ovf-driver	driver for overflow routines (step-mod.F90)
ovf-reg-avgs	computes overflow regional averages
ovf-transports	computes overflow transports
ovf-state	equation of state for overflows
ovf-loc-prd	determine product injection level for product
ovf-F	evaluate overflow forcing term
ovf-UV	set overflow sidewall velocities
ovf-rhs-brtrpc-momentum	renormalize HU for vertical forcing integrals (barotropic.F90)
ovf-brtrpc-renorm	renormalize HU (barotropic.F90)
ovf-rhs-brtrpc-continuity	apply overflow forcing term (barotropic.F90)
ovf-solvers-9pt	compute stencil weights with overflow HU (barotropic.F90)
ovf-HU	adjust vertical depth HU for overflows
ovf-UV-solution	renormalize overflow velocity columns (step-mod.F90)

Appendix E: POP2 OFP Input File

In the POP2 implementation, a simple text file called the overflow input file, specifies the overflow number, parameters and locations in model index coordinates (global indices with first index at 1). We describe the structure and contents of this file here. See Appendix D for relation between overflow input data and POP2 overflow code.

Apart from descriptive comments, the first data line is the total number of overflows. Then follows blocks of lines having the same logical structure, one for each overflow. Each overflow block starts with the number of the overflow, then a character descriptor. The next six lines are parameters specific to each overflow; note that the order is important. We also show the parameter symbol from Section 2A and Table 1 to the right of the parameter description. The next block is for kmt changes; note, first line should be set to 0 if there are no kmt changes; each kmt change is $i, j,$ *old and new* kmt indices. Next block gives the interior, source and entrainment regional average index boundaries, after a blank comment line; each line is $imin, imax, jmin, jmax, kmin, kmax$ (the file structure was written for variable k, but constrained internally for fixed k, so that $kmin = kmax$). Next block is the source grid box (i, j, k) values and sidewall orientation, with the first line the number of gridboxes, followed by each (i, j, k) and orientation value, ordered to increase in i or j, whichever is appropriate. Then follows entrainment grid box (i, j, k) and orientation, similar to source, and finally the product grid boxes. Product grid boxes have one or more sets ordered by increasing k (i.e. depth), one for each group of gridboxes; first the number of product sets, then each set as number, (i, j, k) and orientation. By convention the source (src) and entrainment (ent) grid values refer to the grid box that the overflows flow INTO; product (prd) grid values refer to the grid box from which the overflow flows OUT OF. All indices refer to the POP2 T-grid. All of the overflow grid boxes (i.e. (i, j, k) values) are below the bottom topography but have sidewalls adjacent to active ocean points from which overflow waters flow from or into.

Orientation of overflow sidewalls is specified by an index from 1 to 4, with 1=increasing x direction, 2=increasing y direction, 3=decreasing x direction and 4=decreasing y direction (see Fig. 2). As src,ent always flow INTO an overflow gridbox and prd flows OUT, there should be no ambiguity.

Below we present the POP2 overflow input file for the four overflows from Section 3. We give an example point to illustrate the structure. In Table E1, for the first overflow, the third product point in the second product set has index coordinates $i = 14,\ j = 362,\ k = 44$ and orientation 3. Since 3 is decreasing x for fixed y (see Fig. 2), this means the overflow product proceeds OUT of this box towards decreasing x (i.e. grid direction "west") at level 44, which according to Table C1 has a bottom depth of 1665 m.

Table E1. Overflow Input File for POP2

Values	Description
4	Total number of overflows
1 Denmark Strait	number and name of overflow
65.0	latitude of overflow (degrees) ϕ
5.0E06	width of strait at surface (cm) W_s
450.0E02	upstream source water thickness (cm) h_u
100.0E05	distance from strait to shelf-slope break (cm) x_{ssb}
2.5E-2	bottom slope just over shelf-slope break (unitless) α
3.0E-3	bottom drag coefficient C_d
3	3=number of kmt changes, as (i,j,kmtold,kmtnew)
19 372 33 32	pop up dms src i=19, j=372 kmtold=33 kmtnew=32
19 371 33 32	pop up dms src
19 370 33 32	pop up dms src
	regional (i,j,k) min and max
10 15 360 367 33 33	interior imin=10, imax=15, jmin=360, jmax=367, kmin,max=33
20 30 370 372 33 33	src imin=20, imax=30, jmin=370, jmax=372, kmin=33,kmax=33
12 15 363 367 39 39	ent imin=12, imax=15, jmin=363, jmax=367, kmin,max=39
3	src (i,j,k) orientation, 3= number of points
19 370 33 1	i=19, j=370, k=33, 1=increasing x sidewall, etc....
19 371 33 1	
19 372 33 1	
5	ent (i,j,k) orientation, 5= number of points
16 363 39 3	i=16, j=363, kmt=39, 3=decreasing x sidewall, etc....
16 364 39 3	
16 365 39 3	
16 366 39 3	
16 367 39 3	
7	prd (i,j,k) orientation, number of product sets of points
4	number prd points in set 1
15 360 43 3	
15 361 43 3	
15 362 43 3	
15 363 43 3	

Table E1 continued page 2. Overflow Input File for POP2

Values	Description
4	number prd points in set 2
14 360 44 3	
14 361 44 3	
14 362 44 3	
14 363 44 3	
7	number prd points in set 3
13 359 46 3	
13 360 46 3	
13 361 46 3	
13 362 46 3	
13 363 46 3	
13 364 46 3	
13 365 46 3	
4	number prd points in set 4
12 359 47 3	
12 360 47 3	
12 361 47 3	
12 362 47 3	
6	number prd points in set 5
11 359 48 3	
11 360 48 3	
11 361 48 3	
11 362 48 3	
11 363 48 3	
11 364 48 3	
5	number prd points in set 6
10 359 49 3	
10 360 49 3	
10 361 49 3	
10 362 49 3	
10 363 49 3	
6	number prd points in set 7
7 352 50 3	
7 353 50 3	
7 354 50 3	
7 355 50 3	
7 356 50 3	
7 357 50 3	

Table E1 continued page 3. Overflow Input File for POP2

Values	Description
2 Faroe Bank Channel	number and name of overflow
62.0	latitude of overflow (degrees) ϕ
1.5E06	width of strait at surface (cm) W_s
300.0E02	upstream source water thickness (cm) h_u
250.0E05	distance from strait to shelf-slope break (cm) x_{ssb}
1.5E-2	bottom slope just over shelf-slope break (unitless) α
3.0E-3	bottom drag coefficient C_d
3	3=number of kmt changes, as (i,j,kmtold,kmtnew)
38 349 38 37	pop up fbc src i=38, j=349 kmtold=38 kmtnew=37
38 350 38 37	pop up fbc src
38 351 38 37	pop up fbc src
	regional (i,j,k) min and max
25 30 352 357 38 38	interior imin=25, imax=30, jmin=352, jmax=357, kmin,max=38
39 42 349 355 38 38	src imin=39, imax=42, jmin=349, jmax=355, kmin=38,kmax=38
28 31 352 355 40 40	ent imin=28, imax=31, jmin=352, jmax=355, kmin,max=40
3	src (i,j,k) orientation, 3= number of points
38 349 38 1	i=38, j=349, k=38, 1=increasing x sidewall, etc....
38 350 38 1	
38 351 38 1	
4	ent (i,j,k) orientation, 4= number of points
32 352 40 3	i=32, j=352, k=40, 3=decreasing x sidewall, etc....
32 353 40 3	
32 354 40 3	
32 355 40 3	
6	prd (i,j,k) orientation, number of product sets of points
3	number prd points in set 1
30 352 43 3	
30 353 43 3	
30 354 43 3	
3	number prd points in set 2
29 353 45 3	
29 354 45 3	
29 355 45 3	

Table E1 continued page 4. Overflow Input File for POP2

Values	Description	
3	number prd points in set 3	
28 352 47 3		
28 353 47 3		
28 354 47 3		
4	number prd points in set 4	
26 351 48 3		
26 352 48 3		
26 353 48 3		
26 354 48 3		
3	number prd points in set 5	
23 350 49 3		
23 351 49 3		
23 352 49 3		
4	number prd points in set 6	
20 346 50 3		
20 347 50 3		
20 348 50 3		
20 349 50 3		
3 Ross Sea	number and name of overflow	
75.0	latitude of overflow (degrees)	ϕ
100.0E05	width of strait at surface (cm)	W_s
400.0E02	upstream source water thickness (cm)	h_u
150.0E05	distance from strait to shelf-slope break (cm)	x_{ssb}
3.2E-2	bottom slope just over shelf-slope break (unitless)	α
3.0E-3	bottom drag coefficient	C_d
3	3=number of kmt changes, as (i,j,kmtold,kmtnew)	
198 7 34 33	pop up rss src i=198, j=7 kmtold=34 kmtnew=33	
199 7 34 33	pop up rss src	
200 7 34 33	pop up rss src	
	regional (i,j,k) min and max	
198 200 8 12 34 34	interior imin=198, imax=200, jmin=8, jmax=12, kmin,max=34	
196 200 4 6 34 34	src imin=196, imax=200, jmin=4, jmax=6, kmin=34,kmax=34	
194 196 13 17 40 40	ent imin=194, imax=196, jmin=13, jmax=17, kmin,max=40	

Table E1 continued page 5. Overflow Input File for POP2

Values	Description
3	src (i,j,k) orientation, 3= number of points
198 7 34 4	i=198, j=7, k=34, 4=decreasing y sidewall, etc....
199 7 34 4	
200 7 34 4	
3	ent (i,j,k) orientation, 3= number of points
194 12 40 2	i=194, j=12, kmt=40, 2=increasing y sidewall, etc....
195 12 40 2	
196 12 40 2	
9	prd (i,j,k) orientation, number of product sets of points
3	number prd points in set 1
194 13 43 2	
195 13 43 2	
196 13 43 2	
3	number prd points in set 2
194 14 45 2	
195 14 45 2	
196 14 45 2	
3	number prd points in set 3
194 15 46 2	
195 15 46 2	
196 15 46 2	
3	number prd points in set 4
194 16 47 2	
195 16 47 2	
196 16 47 2	
3	number prd points in set 5
194 17 49 2	
195 17 49 2	
196 17 49 2	
3	number prd points in set 6
194 18 51 2	
195 18 51 2	
196 18 51 2	
3	number prd points in set 7
194 19 52 2	
195 19 52 2	
196 19 52 2	

Table E1 continued page 6. Overflow Input File for POP2

Values	Description
3	number prd points in set 8
198 18 53 1	
198 19 53 1	
198 20 53 1	
3	number prd points in set 9
199 18 54 1	
199 19 54 1	
199 20 54 1	
4 Weddell Sea	number and name of overflow
75.0	latitude of overflow (degrees) ϕ
100.0E05	width of strait at surface (cm) W_s
300.0E02	upstream source water thickness (cm) h_u
150.0E05	distance from strait to shelf-slope break (cm) x_{ssb}
3.2E-2	bottom slope just over shelf-slope break (unitless) α
3.0E-3	bottom drag coefficient C_d
4	4=number of kmt changes, as (i,j,kmtold,kmtnew)
5 9 36 35	pop up wdl src i=5, j=9 kmtold=34 kmtnew=37
6 9 36 35	pop up wdl src
7 9 36 35	pop up wdl src
8 9 36 35	pop up wdl src
	regional (i,j,k) min and max
5 8 10 13 36 36	interior imin=5, imax=8, jmin=10, jmax=13, kmin,max=36
5 8 6 8 36 36	src imin=5, imax=8, jmin=6, jmax=8, kmin=36,kmax=36
1 3 11 13 40 40	ent imin=1, imax=3, jmin=11, jmax=13, kmin,max=40
4	src (i,j,k) orientation, 4= number of points
5 9 36 4	i=5, j=9, k=36, 4=decreasing y sidewall, etc....
6 9 36 4	
7 9 36 4	
8 9 36 4	
3	ent (i,j,k) orientation, 3= number of points
1 10 40 2	i=1, j=10, kmt=40, 2=increasing y sidewall, etc....
2 10 40 2	
3 10 40 2	

Table E1 continued page 7. Overflow Input File for POP2

Values	Description
9	prd (i,j,k) orientation, number of product sets of points
3	number prd points in set 1
318 11 42 2	
319 11 42 2	
320 11 42 2	
3	number prd points in set 2
317 12 43 2	
318 12 43 2	
319 12 43 2	
3	number prd points in set 3
316 13 45 2	
317 13 45 2	
318 13 45 2	
3	number prd points in set 4
315 14 47 2	
316 14 47 2	
317 14 47 2	
3	number prd points in set 5
315 15 49 2	
316 15 49 2	
317 15 49 2	
3	number prd points in set 6
315 16 51 2	
316 16 51 2	
317 16 51 2	
3	number prd points in set 7
315 17 53 2	
316 17 53 2	
317 17 53 2	
3	number prd points in set 8
315 20 54 1	
315 21 54 1	
315 22 54 1	
3	number prd points in set 9
317 21 55 1	
317 22 55 1	
317 23 55 1	

Appendix F: POP2 OFP Restart File

The OFP implementation into POP2 requires a text restart file to ensure exact restarts. This text file consists of much of the parametric and indexical data from the overflow input file of Appendix E. Additionally, there are a number of secondary indices based on overflow orientation needed to compute regional tracer means and product path densities. Also, one key index relates to the product injection level of the previous time step (i.e. a relative product set index- see Appendix E). A typical overflow restart file is too lengthy to be included here, but as it is a text file, it is somewhat self-describing.

Appendix G: Glossary of Acronyms

Term	Description
CCSM	Community Climate System Model
DMS	(or dms) Denmark Strait
ent	referring to the entrainment region, sidewall or transport
ETOPO5	Earth Topography at 5 minute resolution
FBC	(or fbc) Faroe Bank Channel
TO	Table of Observations of Legg et al. (2008)
GIS	Greenland-Iceland-Scotland
GM	Gent/McWilliams parameterization of eddy transport
gx1	CCSM ocean/sea ice grid, Greenland pole at nominal 1° resolution
int	referring to the interior region
OGCM	Ocean General Circulation Model
OFP	Overflow Parameterization
POP1.4	Parallel Ocean Program, Version 1.4
POP2	Parallel Ocean Program, Version 2
prd	referring to the product injection depth, sidewall or transport
src	referring to the source region, sidewall or transport
RSS	(or rss) Ross Sea
WDL	(or wdl) Weddell Sea
WLK	referring to Whitehead et al. (1974)

References

Bryan, F. O., G. Danabasoglu, N. Nakashiki, Y. Yoshida, D.-H. Kim, J. Tsutsui, and S. C. Doney, 2006: Response of the North Atlantic thermohaline circulation and ventilation to increasing carbon dioxide in CCSM3. *J. Climate*, **19**, 2382-2397.

Born, A. et al., 2008: Sensitivity of the Atlantic ocean circulation to a hydraulic overflow parameterisation in a coarse resolution model: Response of the subpolar gyre, *Ocean Modeling*, doi:10.1016/j.ocemod.2008.11.006

Dickson, R. R., and J. Brown, 1994: The production of North Atlantic Deep Water: Sources, rates and pathways, *J. Geophys. Res.*, **99**, No. C6, 12319–12341.

Dye, S., B. Hansen, S. Osterhus, D. Quadfasel, B. Rudels, 2007: The overflow of dense water across the Greenland-Scotland Ridge, *CLIVAR Exchanges*, **12**, No.1, 20–22.

Girton, J. B., L. J. Pratt, D. A. Sutherland, and J. F. Price, 2006: Is the Faroe Bank Channel Overflow Hydraulically Controlled? *J. Phys. Ocean.*, **36**, Notes and Correspondence 2340–2349.

Griffies, S. M., C. Boning, F. O. Bryan, E. P. Chassignet, R. Gerdes, H. Hasumi, A. Hirst, A. Treguier, D. Webb, 2000: Developments in ocean climate modeling, *Ocean Modelling*, **2**, 123–192.

Griffies, S. M., 2003: Fundamentals of Ocean Climate Models, Princeton University Press, pp.495.

Kosters, F., 2004: Denmark Strait overflow: Comparing model results and hydraulic transport estimates, *J. Geophys. Res.*, **109**, doi:10.1029/2004JC002297.

Kosters, F., R. H. Kase, A. Schmittner and P. Herrmann, 2005: The effect of Denmark Strait overflow on the Atlantic Meridional Overturning Circulation, *Geophys. Res. Let.*, **32**, L04602, doi:10.1029/2004GL022112.

Legg, S., B. P. Briegleb, Y. Chang, E. P. Chassignet, G. Danabasoglu, T. Ezer, A. L. Gordon, S. Griffies, R. Hallberg, L. Jackson, W. Large, T. Ozgokmen, H. Peters, J. Price, U. Riemenschneider, W. Wu, X. Xu, J. Yang, 2009: Improving oceanic overflow reperesentation in climate models: the Gravity Current Entrainment Climate Process Team, BAMS, May 2009, pp. 657–670.

Levitus, S., T. Boyer, M. Conkright, D. Johnson, T. O'Brien, J. Antonov, C. Stephens, R. Gelfeld, 1998: World ocean database 1998, vol. I: Introduction. NOAA Atlas NESDIS 18, US Government Printing Office, Washington, DC, pp. 346.

Macrander, A., R. H. Kase, U. Send, H. Valdimarsson, S. Jonsson, 2007: Spatial and temporal structure of the Denmark Strait Overflow revealed by acoustic observations, *Ocean Dynamics*, **57**, 75–89.

Price, J. F. and M. O'Neil Baringer, 1994: Outflows and Deep Water Production by

Marginal Seas, *Prog. Oceanog.*, **33**, 161–200.

Price, J. F. and J. Yang, 1998: Marginal Sea Overflows for Climate Simulations, in Ocean Modeling and Parameterization, 155-170, E.P.Chassignet and J. Verron (eds.), Kluwer Academic Publishers. Printed in the Netherlands.

Riemenschneider, U. and S. Legg, 2006: Regional Simulations of the Faroe Bank Channel Overflow in a Level Model, Submitted to Ocean Modelling, 7 September 2006

Roberts, M. J., and R. A. Wood, 1997: Topographic sensitivity studies with a Bryan-Cox-Type ocean model. *J. Phys. Oceanogr.*, **27**, 823-836.

Roberts, M. J., R. Marsh, A. L. New, and R. A. Wood, 1996: An intercomparison of a Bryan-Cox-Type ocean model and an isopycnic ocean model. Part I: The subpolar gyre and high-latitude processes. *J. Phys. Oceanogr.*, **26**, 1495-1527.

Smith, R. D., and Coauthors, 2010: Parallel Ocean Program (POP) reference manual, Ocean component of the Community Climate System Model (CCSM). *Tech. Rep. LA-UR-10-xxxx*, Los Alamos National Laboratory, Los Alamos, NM, XX pp.

Steele, M., R. Morley, W. Ermold, 2001: PHC: a global ocean hydrography with a high-quality Arctic Ocean. *Journal of Climate*, **14**, 2079–2087.

Whitehead, J. A., A. Leetmaa, R. A. Knox, 1974: Rotating Hydraulics of Strait and Sill Flows, *Geophysical Fluid Dynamics*, **6**, 101–125.

Whitehead, J. A., 1989: Internal Hydraulic Control in Rotating Fluids- Applications to Oceans, *Geophys. Astrophys. Fluid Dynamics*, **48**, 169–192.

Winton, M., R. Hallberg, and A. Gnanadesikan, 1998: Simulation of density-driven frictional downslope flow in z-coordinate ocean models. *J. Phys. Oceanogr.*, **28**, 2163-2174.

Wu, W., G. Danabasoglu, W. G. Large, 2007: On the effects of parameterized Mediterranean overflow on North Atlantic ocean circulation and climate, *Ocean Modeling*, **19**, 31–52.

Figure 1. A schematic of the Nordic Seas overflows. T, S, ρ, and M represent temperature, salinity, density, and volume transport, respectively. The subscripts i, s, e, and p indicate interior, source, entrainment, and product water properties, respectively. d is depth, h_u is the upstream thickness of the source water, h_s is the source thickness in the channel, W_s is the width of the channel, α is the maximum slope of the continental shelf near the shelf break, C_d is the bottom drag coefficient, and x_{ssb} is the distance from the sill to the shelf break. The green box shows the raised bottom topography. The thick, short arrows indicate flow directions. The other colored boxes (apart from the product) represent the regions whose T and S are used to compute the necessary densities. The product injection depth shows where the product waters of properties T_p, S_p are injected. See Section 2A for further details.

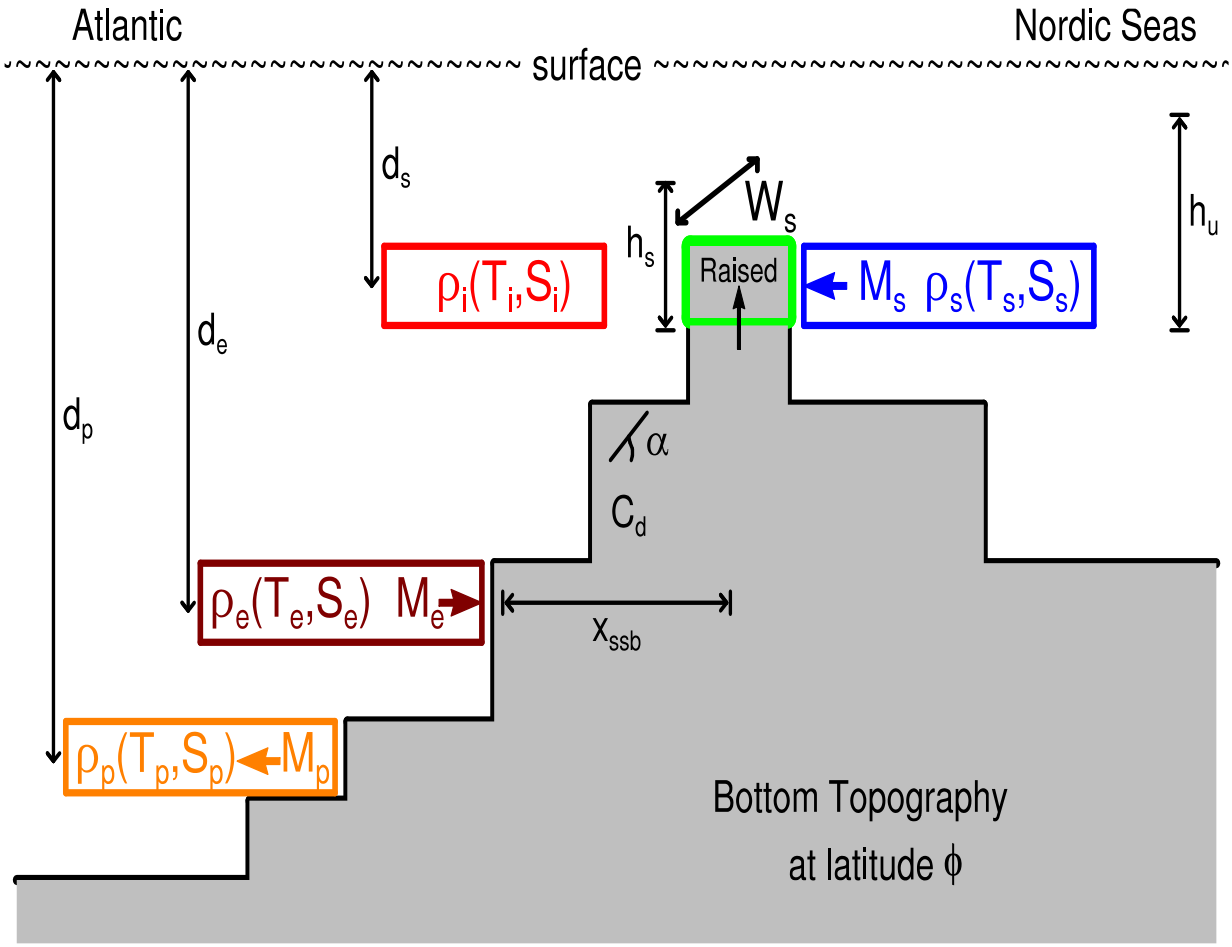

Figure 2. Schematics of T-grid box looking down. A. T-grid boxes at a fixed vertical level k. (i, j) refers to the grid box shown, while the four adjacent box indices are indicated also. Numerals on the four box faces are orientation indices for the overflows. B. T-grid box showing the U-grid corner indices. C. T-grid boxes showing sidewall velocities. Example source overflow, oriented east-to-west in grid space. The overflow velocity vectors, along with the grid dimensions dy, are also shown. If dz_k is the vertical depth of the three T-grid boxes, then the cross sectional areas for the overflows are $dy_{(i,j)}\ dz_k$ and $dy_{(i,j-1)}\ dz_k$. In this example, if M_s is the source transport, then $U_{(i,j,k)} = M_s/(2dy_{(i,j)}dz_k)$ and $U_{(i,j-1,k} = M_s/(2dy_{(i,j-1)}dz_k)$.

A.

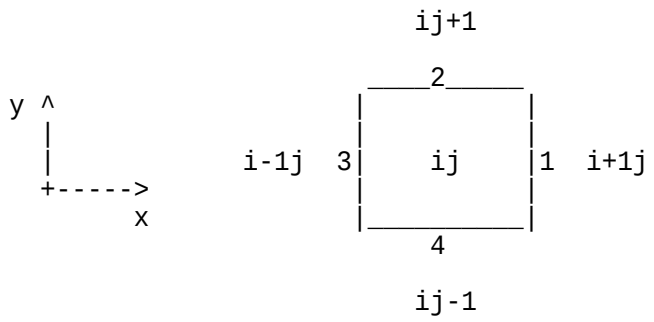

B.

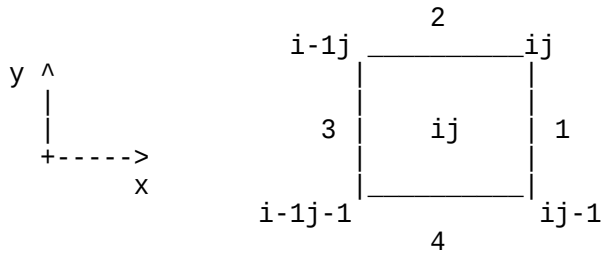

C.

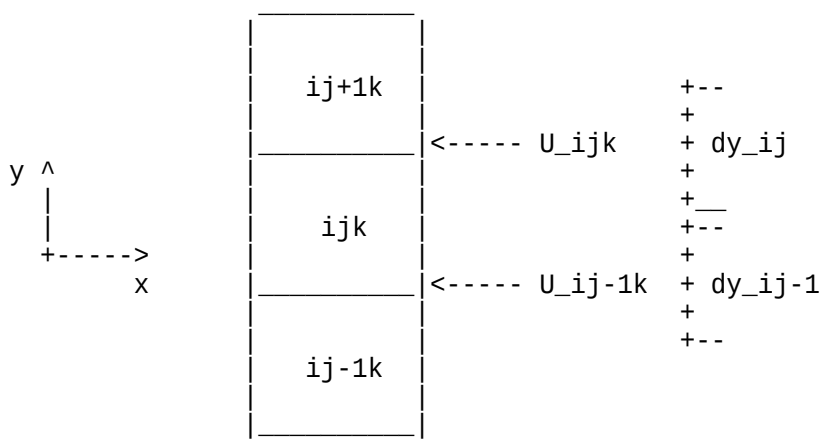

Figure 3. Schematic cross section showing overflows into and out of the bottom topography. S = source, E = entrainment, P = product. Overflow columns for adjustment of baroclinic velocity are shown, as well as the columns where the overflow forcing term F is added to the barotropic equation. The horizontal arrows for the adjusted columns show the direction of the adjustment.

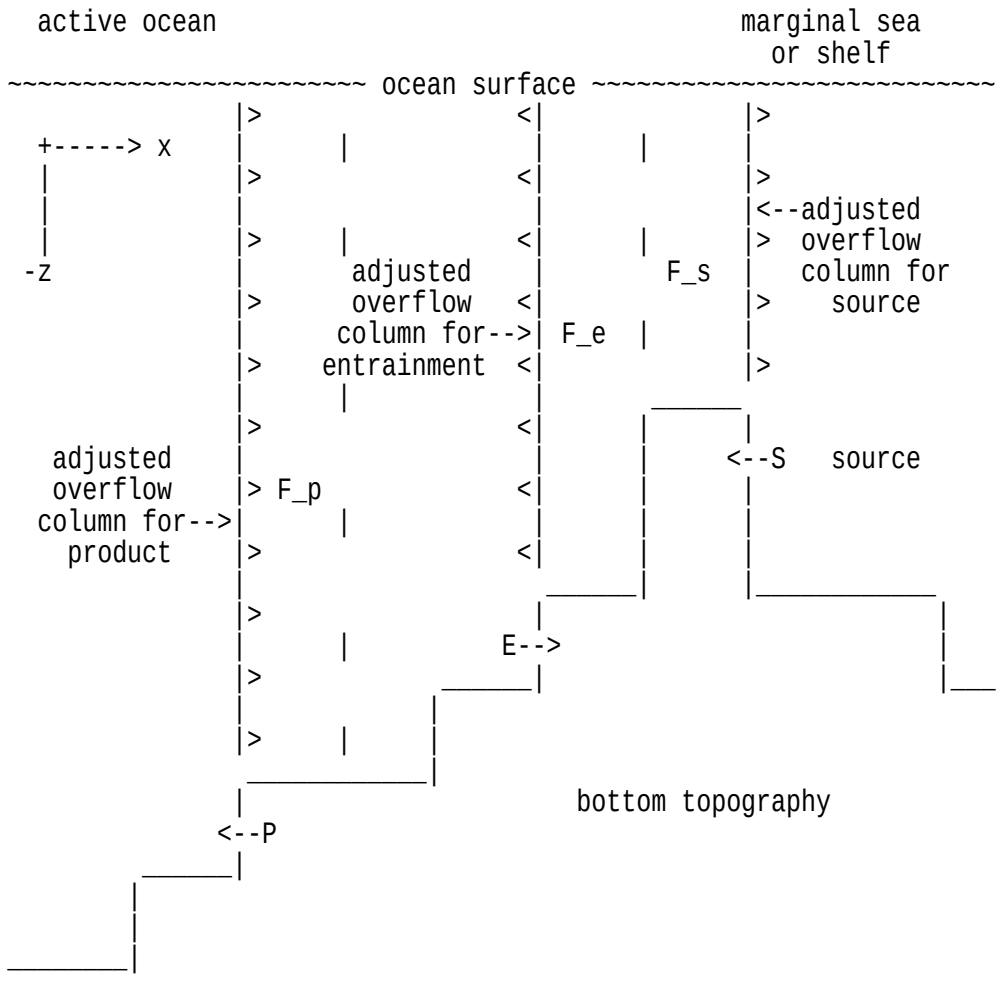

Figure 4a. Greenland-Iceland-Scotland Ridge Topography down to 2000m. Top panel is the POP2 gx1 topography, while the lower panel is the ETOPO5 topography at 5' resolution.

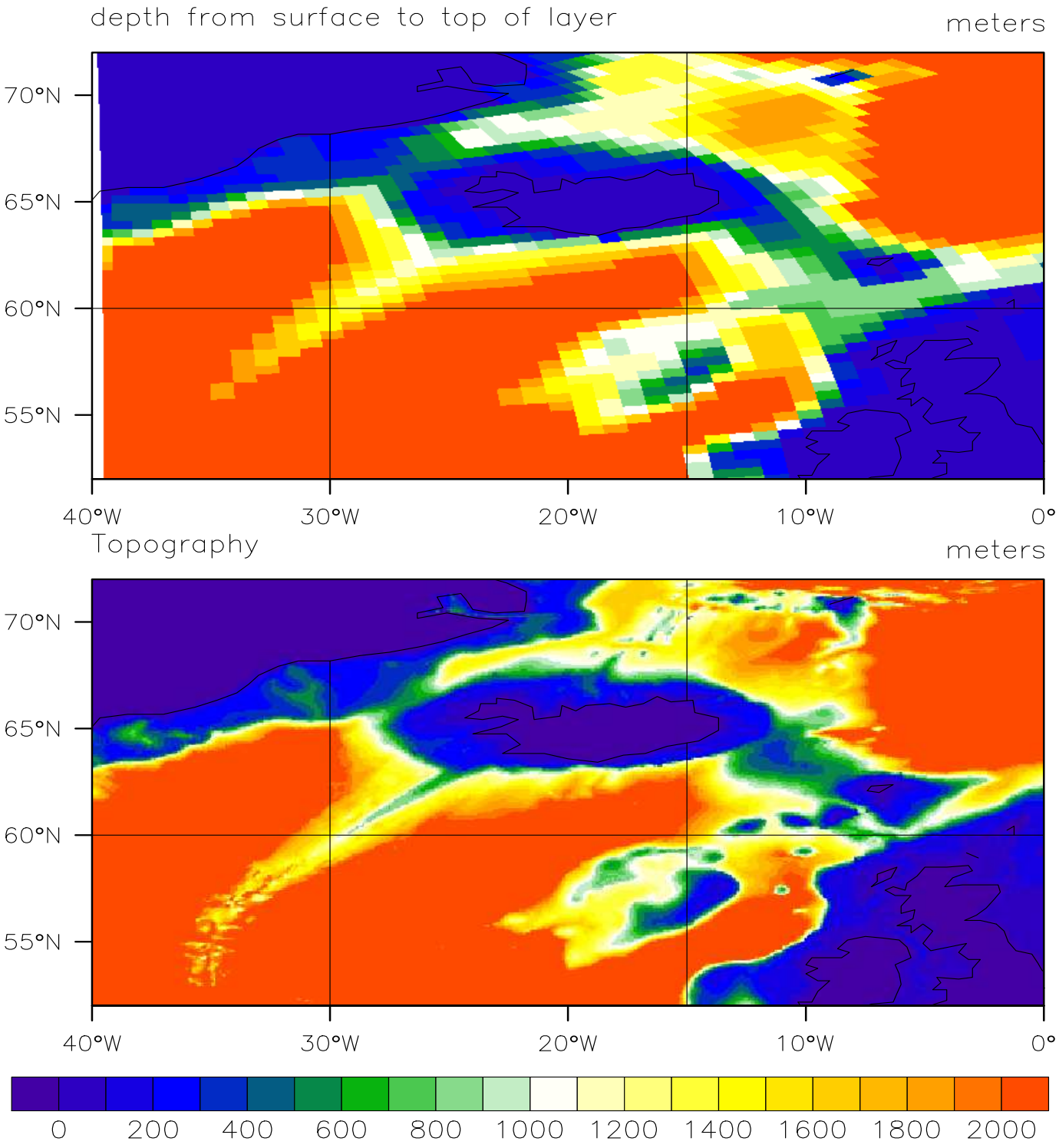

Figure 4b. Greenland-Iceland-Scotland Ridge Topography down to 4000m. Top panel is the POP2 gx1 topography, while the lower panel is the ETOPO5 topography at 5' resolution.

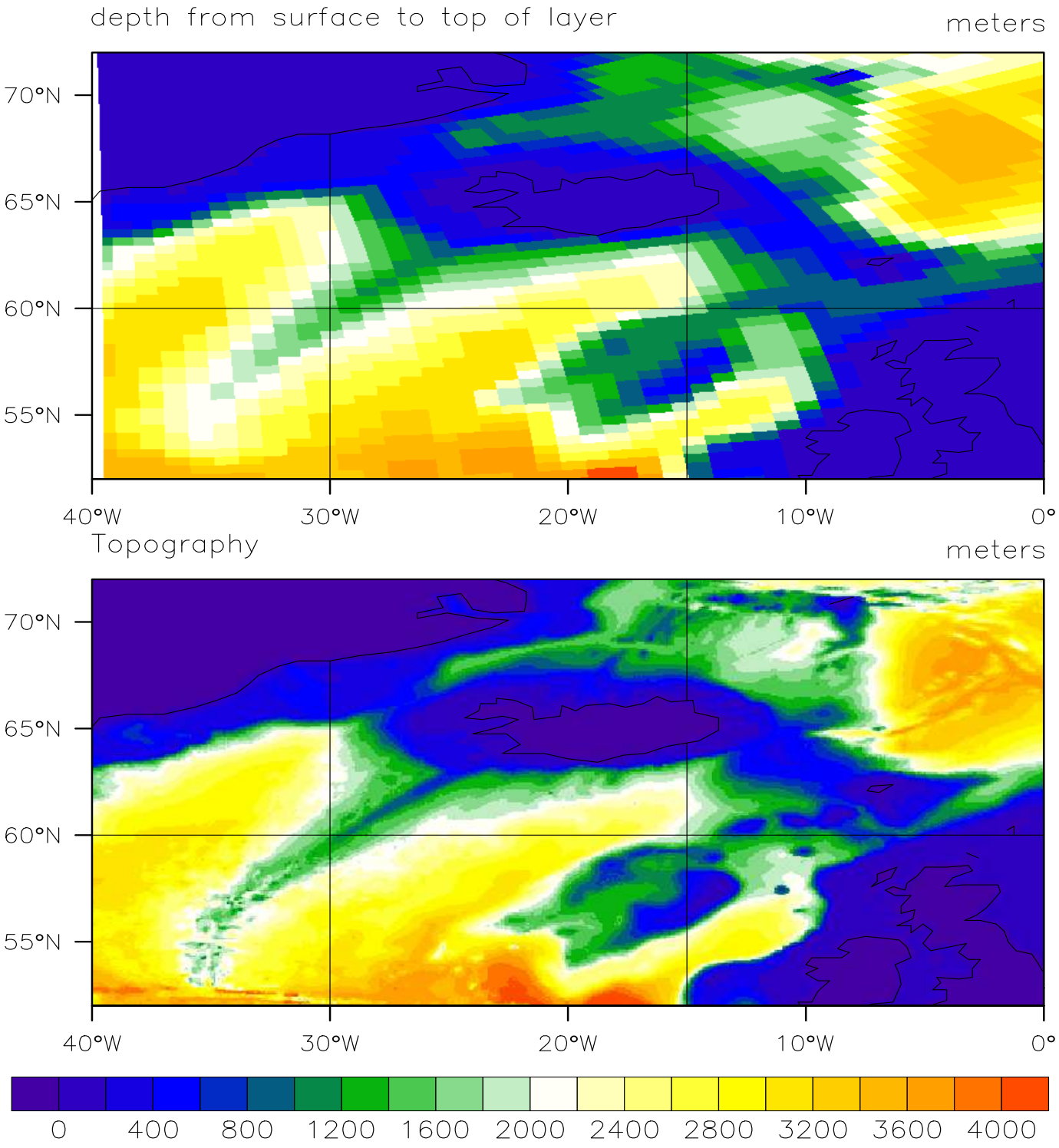

Figure 5a. Ross Sea Topography down to 1000m. Top panel is the POP2 gx1 topography, while the lower panel is the ETOPO5 topography at 5' resolution.

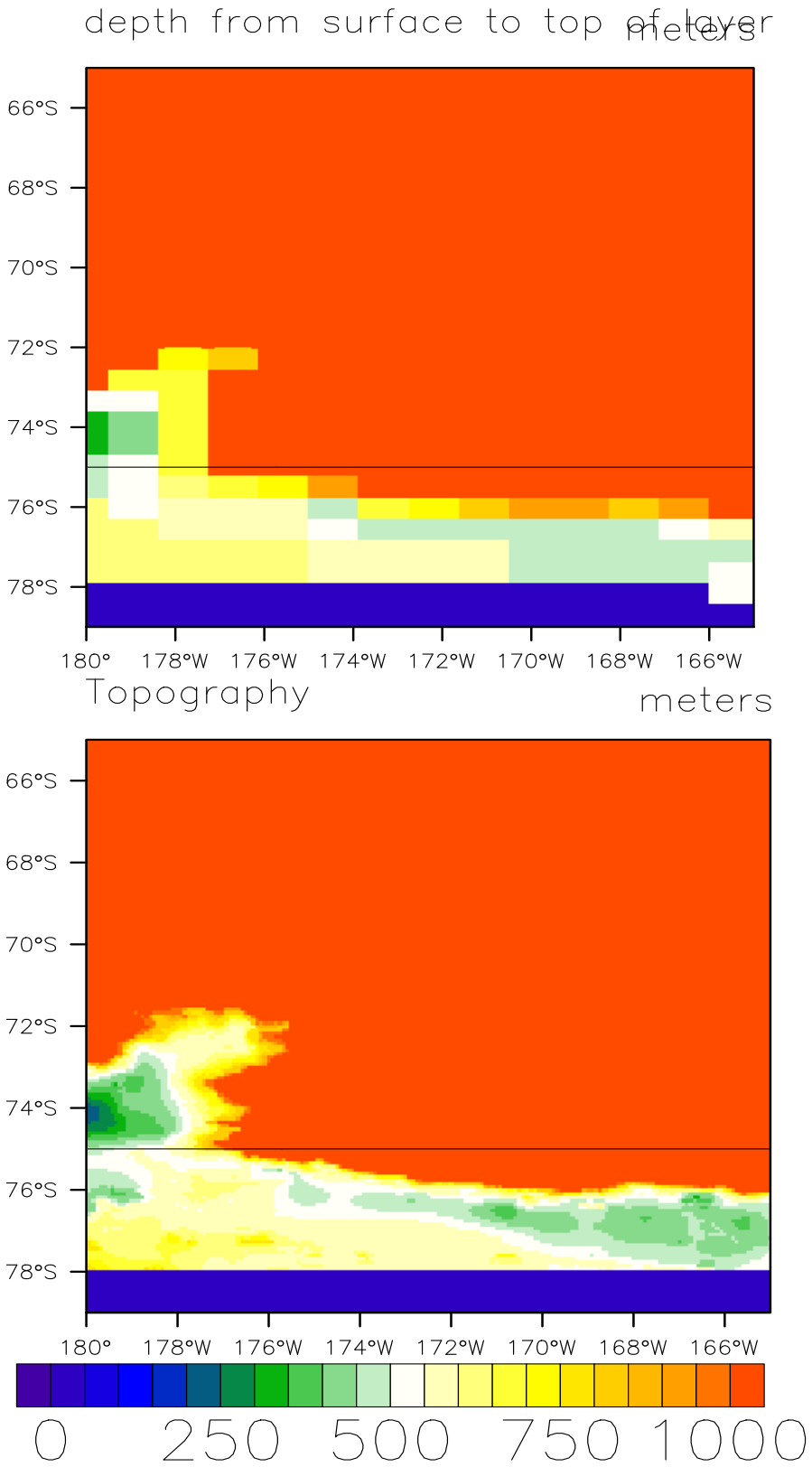

Figure 5b. Ross Sea Topography down to 4000m. Top panel is the POP2 gx1 topography, while the lower panel is the ETOPO5 topography at 5' resolution.

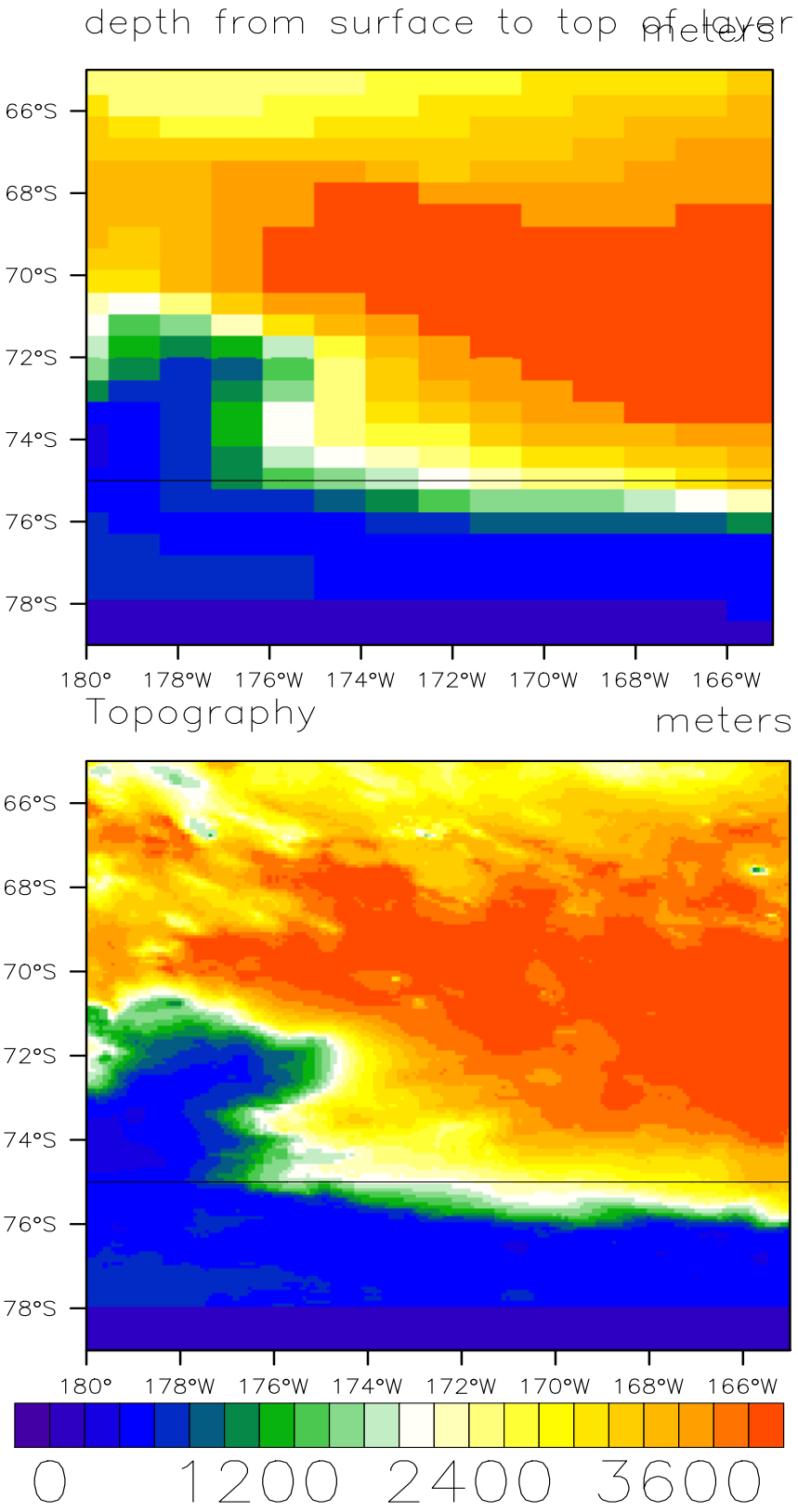

Figure 6a. Weddell Sea Topography down to 1000m. Top panel is the POP2 gx1 topography, while the lower panel is the ETOPO5 topography at 5' resolution.

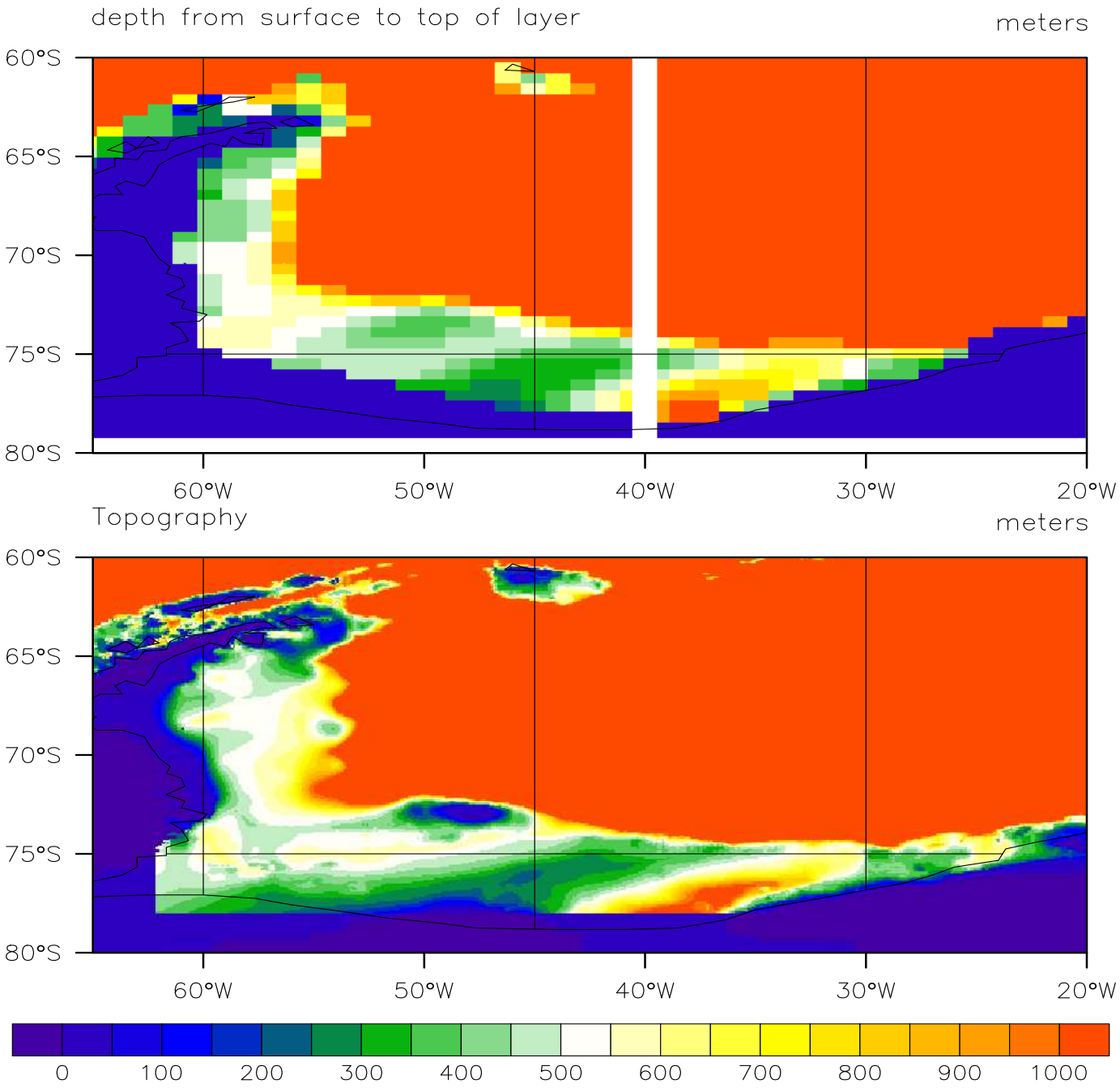

Figure 6b. Weddell Sea Topography down to 4000m. Top panel is the POP2 gx1 topography, while the lower panel is the ETOPO5 topography at 5' resolution.

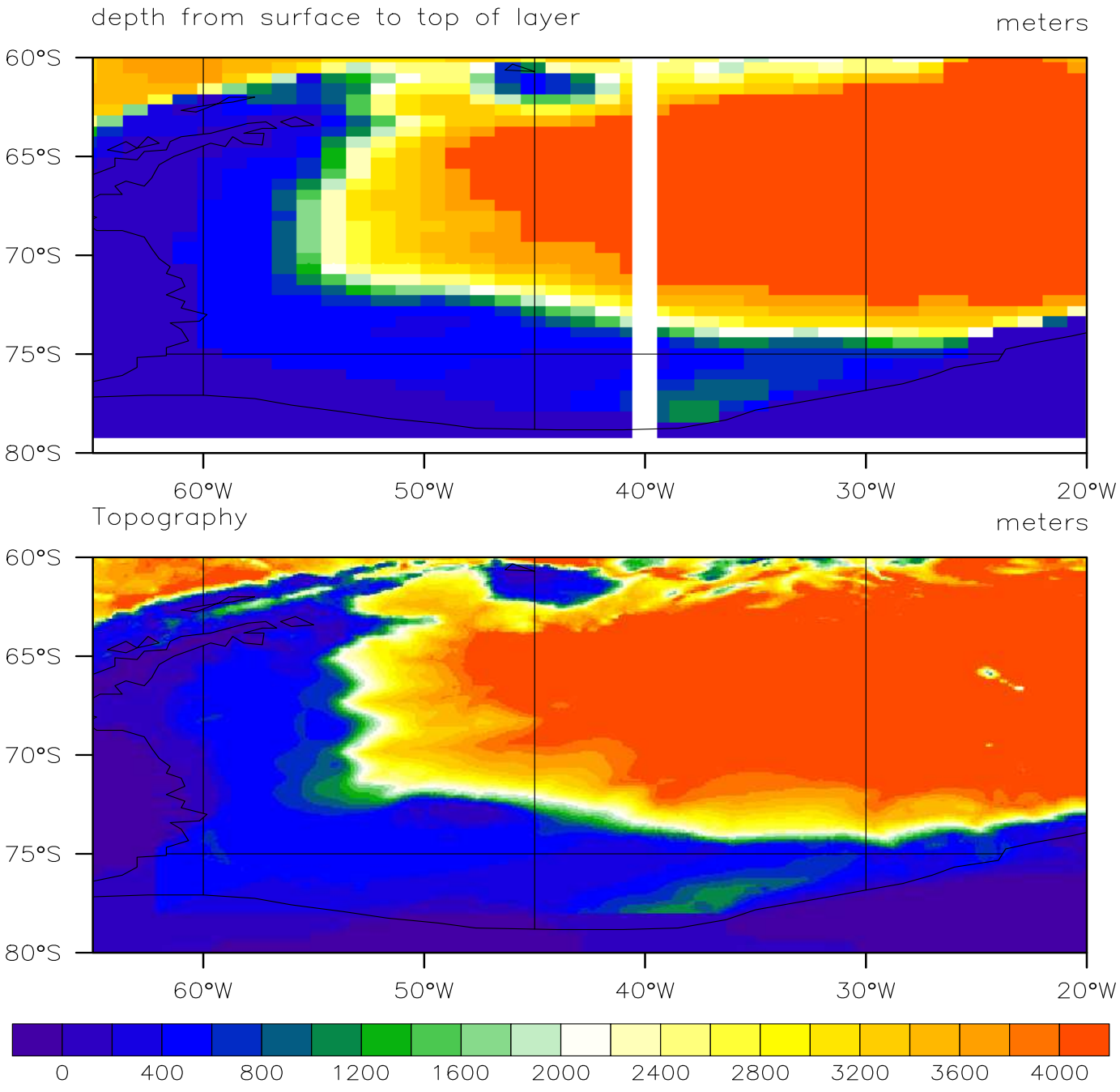

Figure 7a. Bottom topography as represented in the model in the vicinity of the Denmark Strait (DMS) and Faroe Bank Channel (FBC) overflows. The colors indicate the model vertical levels. The corresponding depths are given above the color bar. The boxed regions denoted by I, E, and S indicate the Interior, Entrainment (thin box), and Source regions in the horizontal, respectively, whose temperature and salinity properties are used to compute the necessary densities. The source and entrainment box edges at which the respective water properties and transports are imposed as side boundary conditions in the OGCM are indicated by the black arrows, showing directions corresponding to flows out of the OGCM domain. The white lines denoted by P show the prespecified product water injection locations into the OGCM domain. All product water sites have the same injection direction as denoted by the white arrows drawn at only a few of the sites for clarity.

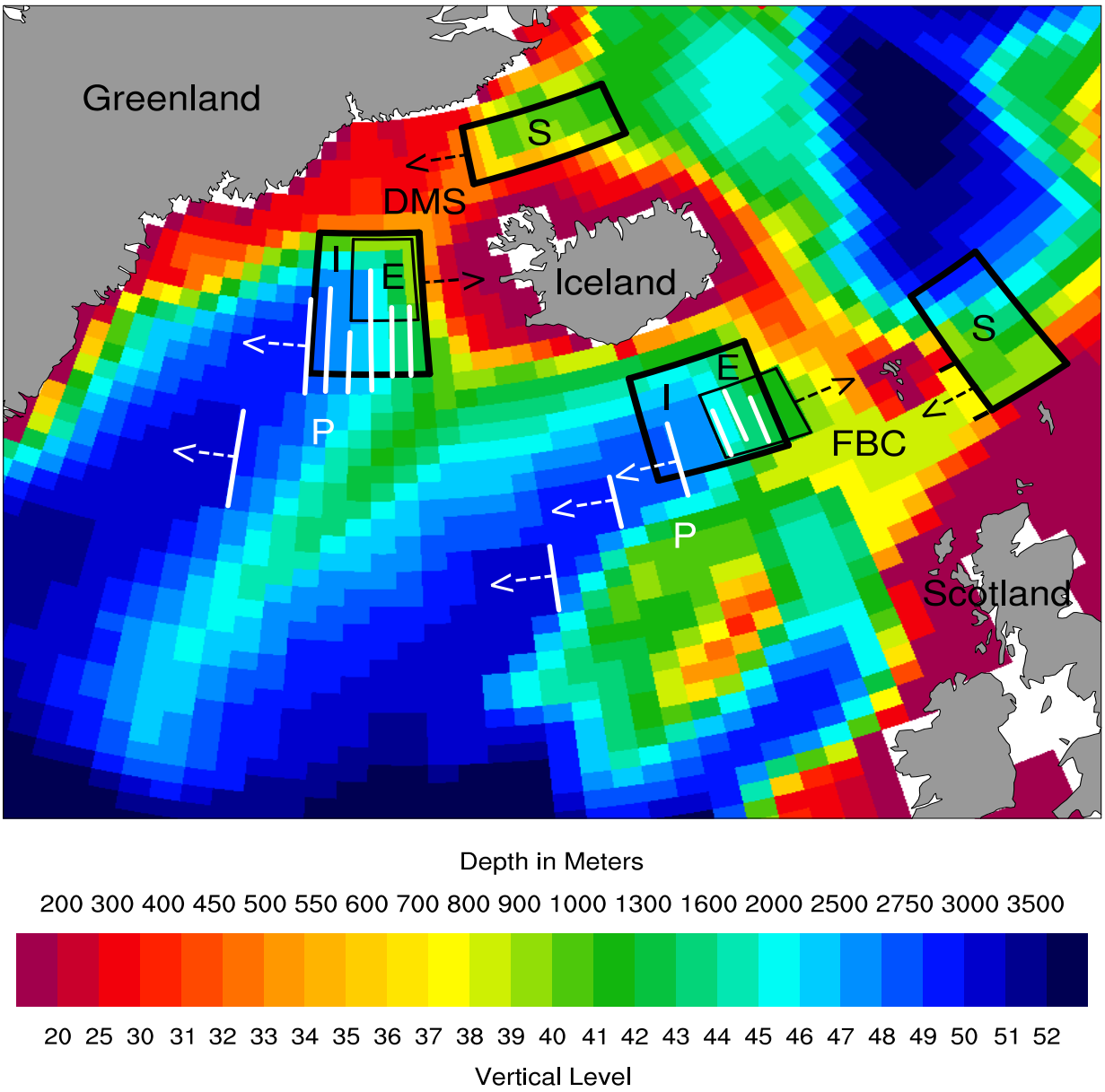

Figure 7b. Greenland-Iceland-Scotland ridge using the x1 resolution ocean topography, with continents in grey. Denmark Strait (DMS) and Faroe Bank Channel (FBC) overflow regions shown. Grid boxes included in the regional averages are: (1) DMS Interior, (2) DMS Source, (3) DMS Entrainment, (4) FBC Interior, (5) FBC Source and (6) FBC Entrainment. Where interior regiona overlies the entrainment region both numbers appear in the same box.

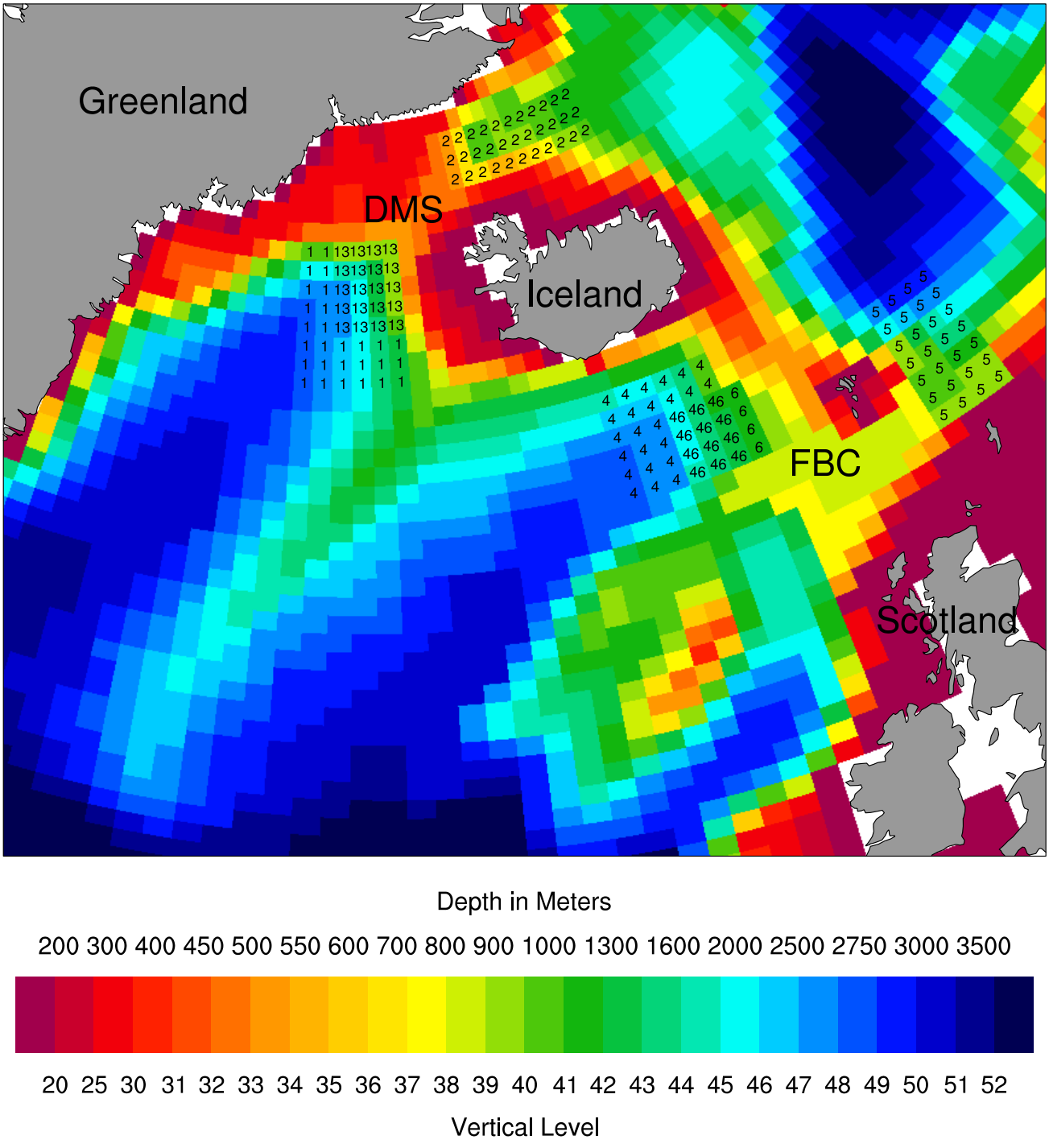

Figure 7c. Greenland-Iceland-Scotland ridge using the x1 resolution ocean topography, with continents in grey. Denmark Strait (DMS) and Faroe Bank Channel (FBC) overflow regions shown. Source (S), entrainment (E) and various product (P) grid boxes shown using their vertical levels.

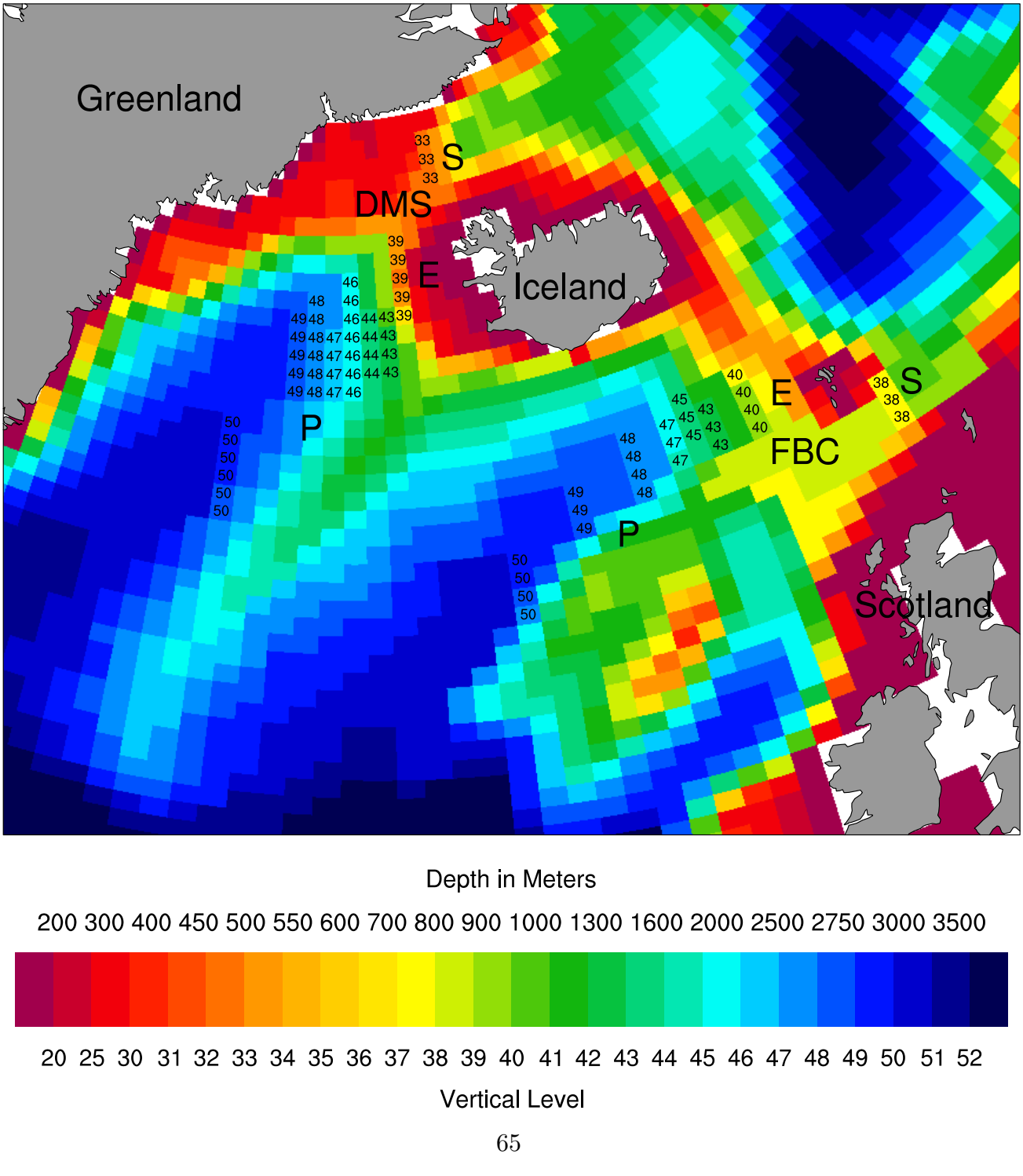

Figure 7d. Bottom topography as represented in the model around Antarctica. The colors indicate the model vertical levels. The corresponding depths are given above the color bar. Antarctic locations of the Ross Sea and Weddell Sea overflows are marked with black arrows, extending from the shelf source across the shelf sill.

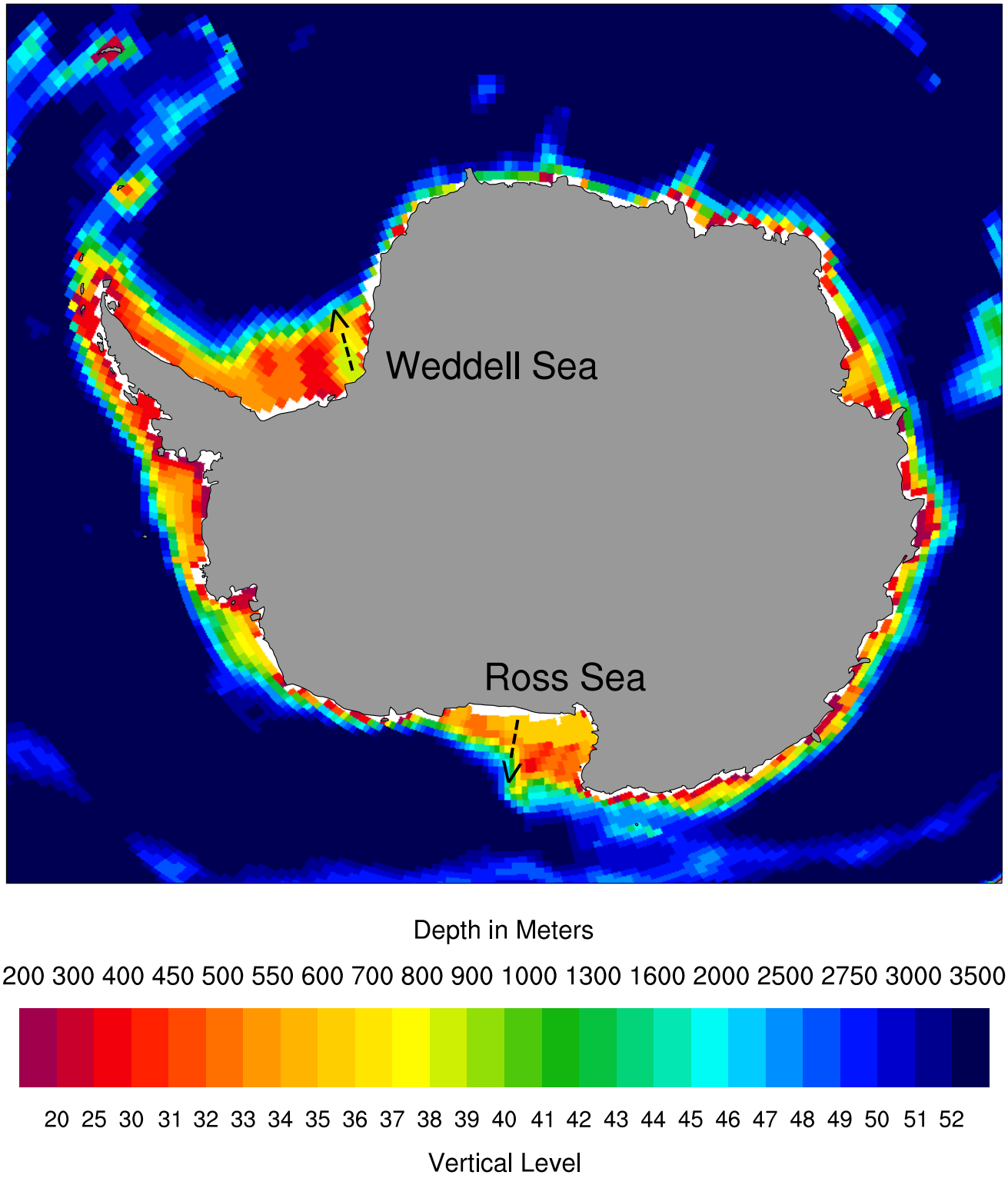

Figure 7e. Bottom topography as represented in the model in the Ross Sea. The colors indicate the model vertical levels. The corresponding depths are given above the color bar. The boxed regions denoted by I, E, and S indicate the Interior, Entrainment (thin box), and Source regions in the horizontal, respectively, whose temperature and salinity properties are used to compute the necessary densities. The source and entrainment box edges at which the respective water properties and transports are imposed as side boundary conditions in the OGCM are indicated by the black arrows, showing directions corresponding to flows out of the OGCM domain. The white lines denoted by P show some of the prespecified product water injection locations into the OGCM domain.

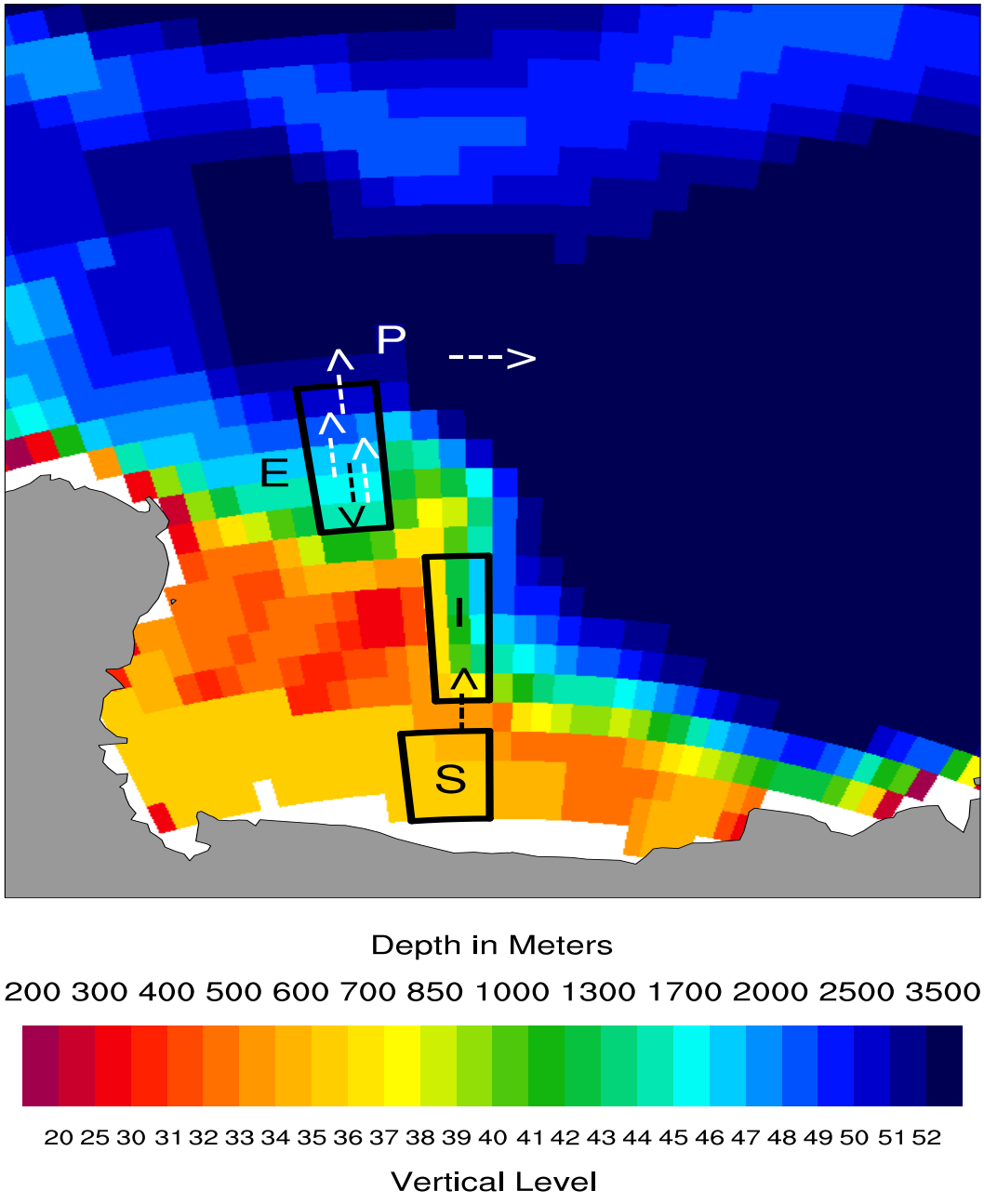

Figure 7f. Bottom topography as represented in the model in the Weddell Sea. The colors indicate the model vertical levels. The corresponding depths are given above the color bar. The boxed regions denoted by I, E, and S indicate the Interior, Entrainment (thin box), and Source regions in the horizontal, respectively, whose temperature and salinity properties are used to compute the necessary densities. The source and entrainment box edges at which the respective water properties and transports are imposed as side boundary conditions in the OGCM are indicated by the black arrows, showing directions corresponding to flows out of the OGCM domain. The white lines denoted by P show some of the prespecified product water injection locations into the OGCM domain.

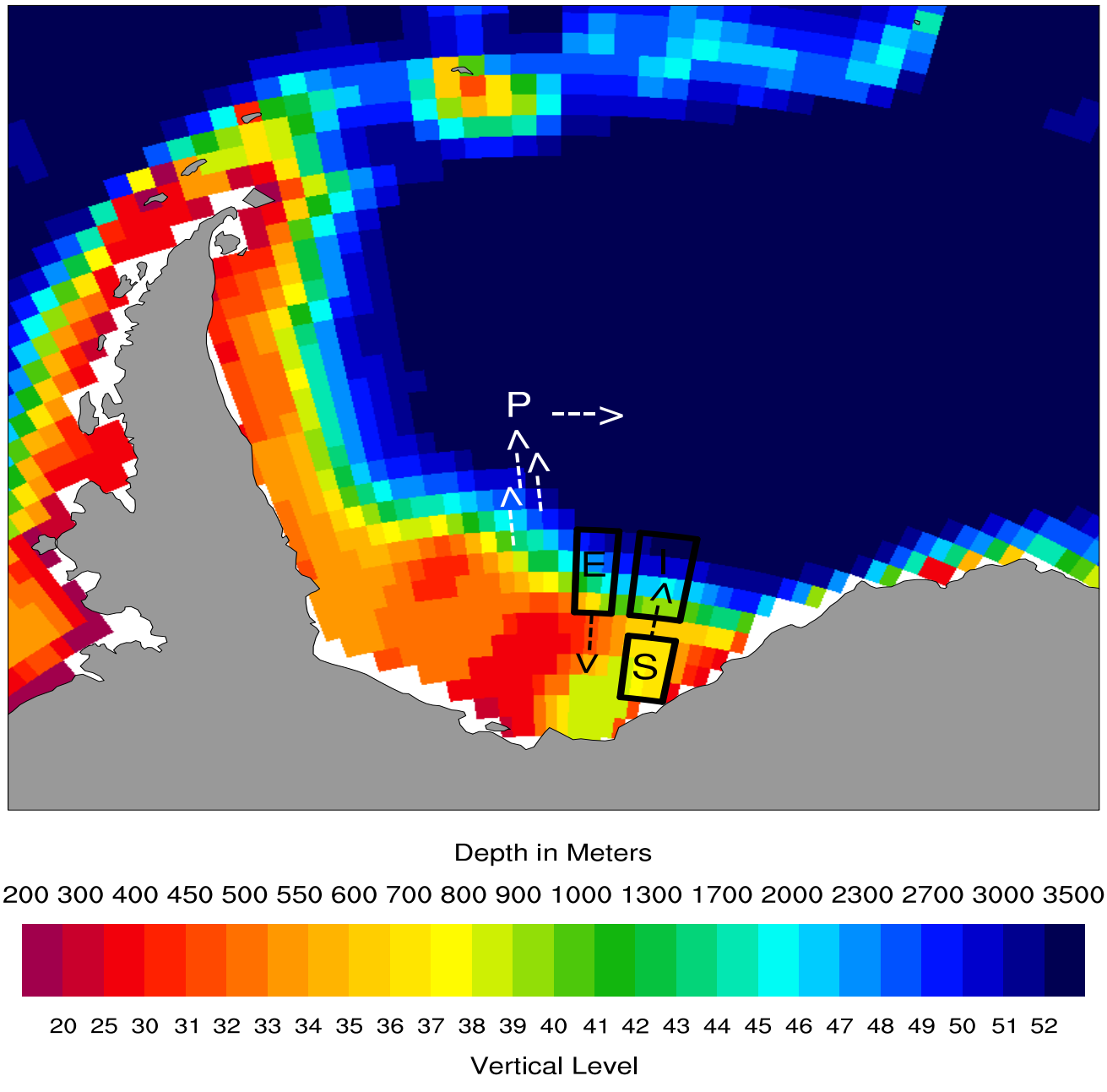

Figure 8. Denmark Strait interior and source vertical density profile (relative to z=0). Regional mean temperature and salinity from Levitus annual observed data (interpolated to the horizontal (gx1) and vertical grid of POP2), are used to compute density at each level. Interior is solid red line and source dashed green line. Channel depth noted and marked by +++++, along with approximate isodensity level and the chosen source thickness h_u shown inbetween.

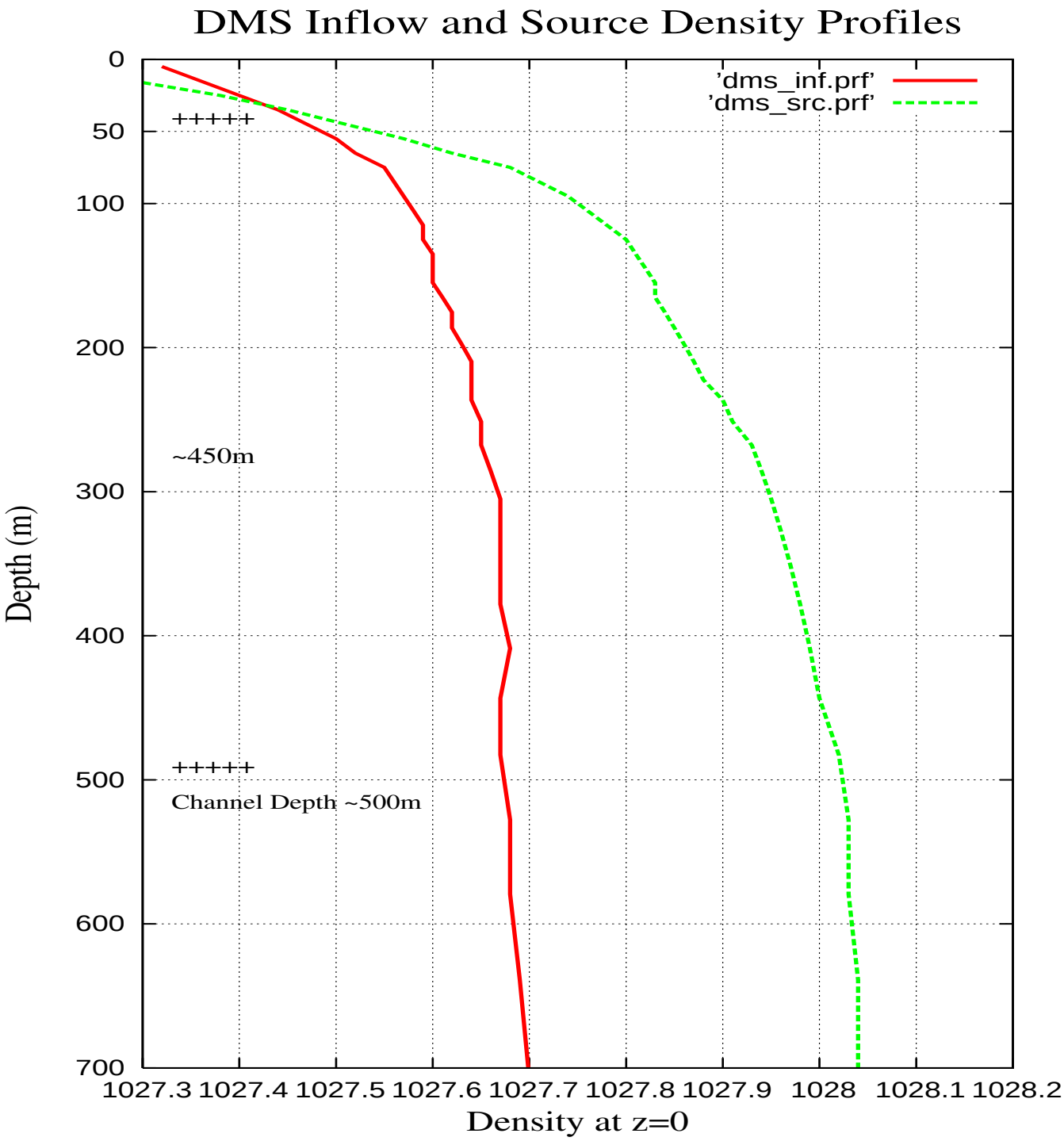

Figure 9. Faroe Bank Channel interior and source vertical density profile (relative to z=0). Regional mean temperature and salinity from Levitus annual observed data (interpolated to the horizontal (gx1) and vertical grid of POP2), are used to compute density at each level. Interior is solid red line, the west source dashed green line, and the east source dashed blue line. Channel depth noted and marked by +++++, along with approximate isodensity level and the source thickness h_u shown inbetween for the west source.

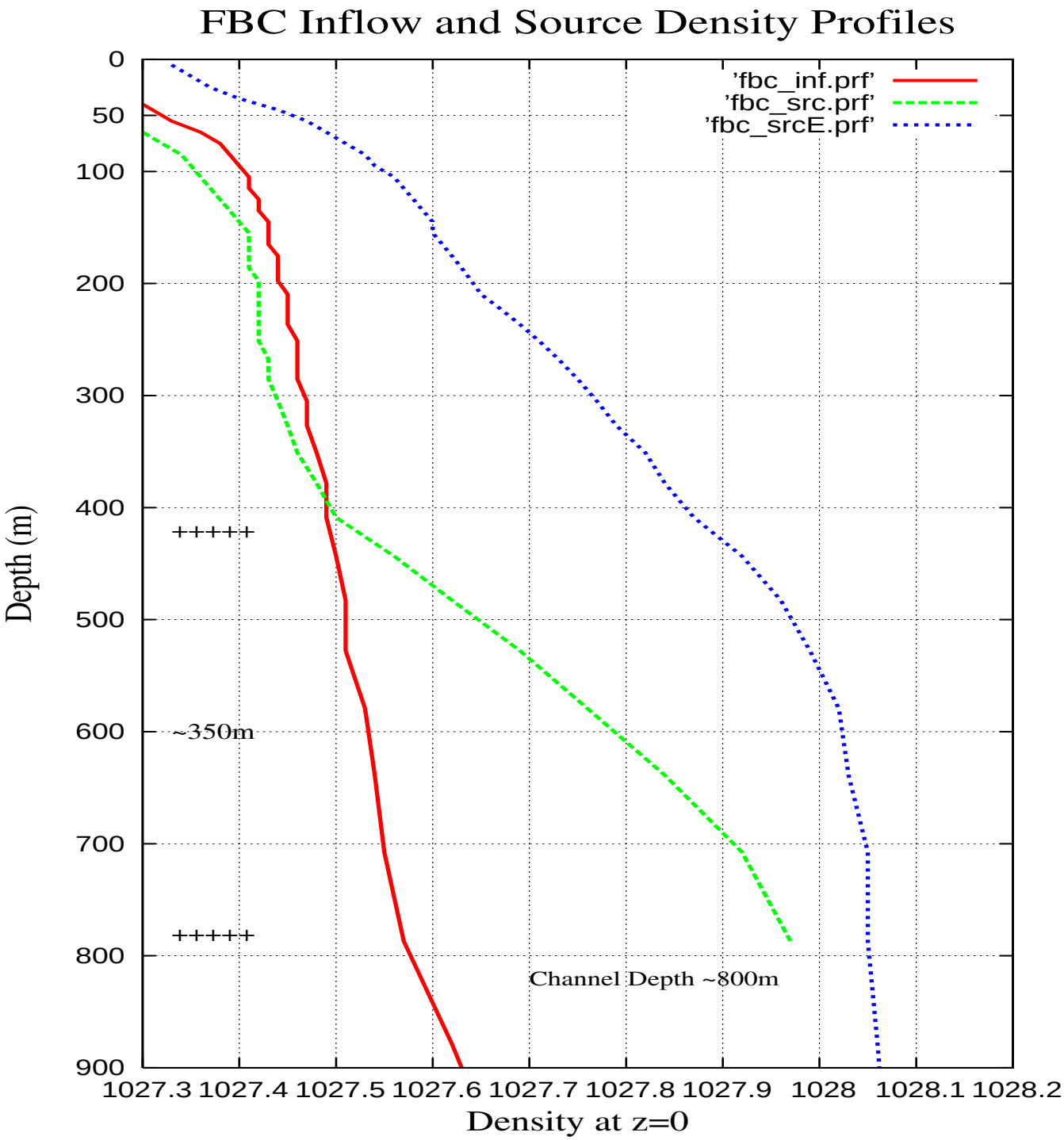

Figure 10. Ross Sea interior and source vertical density profile (relative to z=0). Regional mean temperature and salinity from Levitus annual observed data (interpolated to the horizontal (gx1) and vertical grid of POP2), are used to compute density at each level. Interior is solid red line and source dashed green line. Channel depth noted and marked by $+++++$, along with approximate isodensity level and the chosen source thickness h_u shown inbetween.

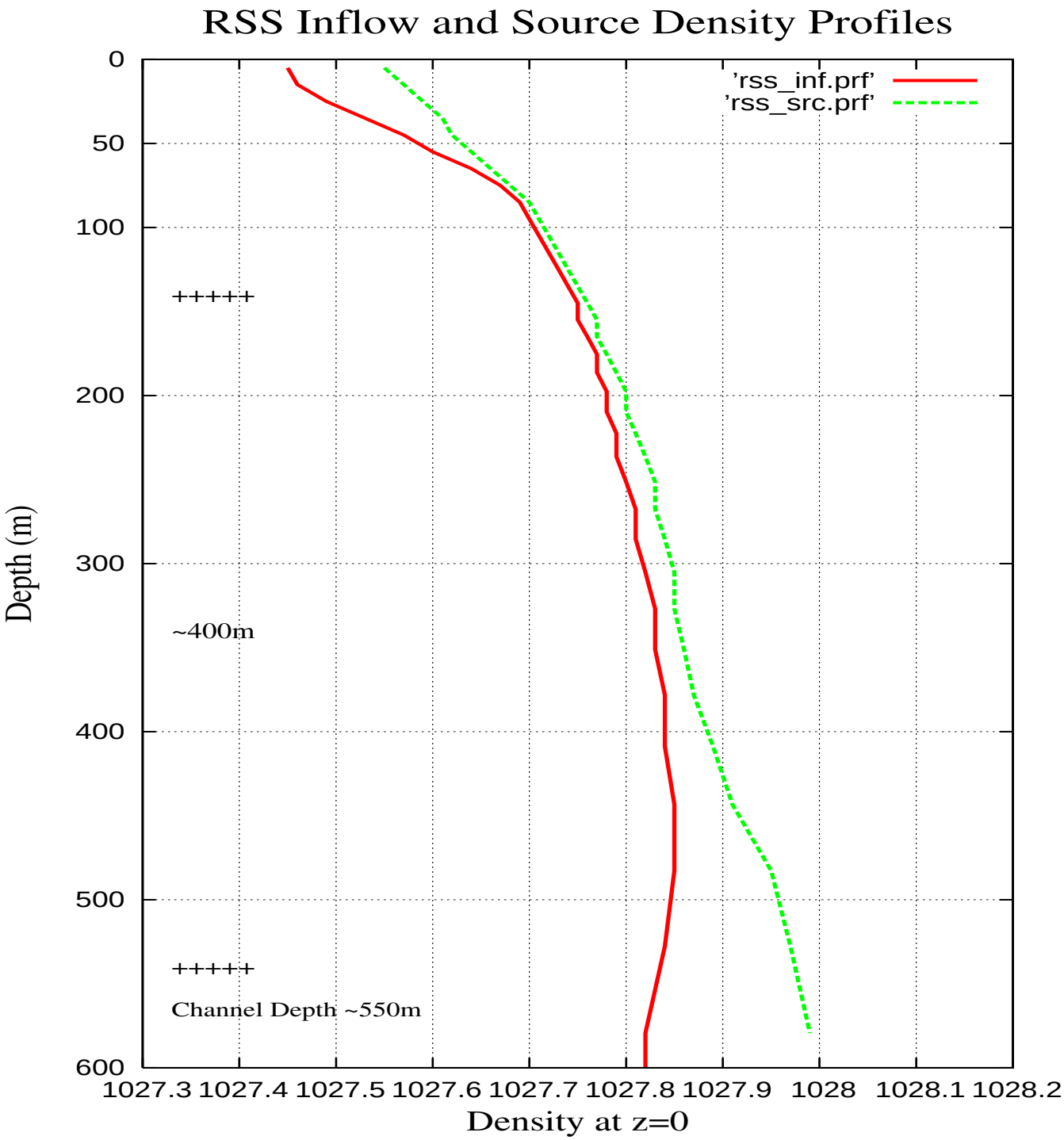

Figure 11. Weddell Sea interior and source vertical density profile (relative to z=0). Regional mean temperature and salinity from Levitus annual observed data (interpolated to the horizontal (gx1) and vertical grid of POP2), are used to compute density at each level. Interior is solid red line and source dashed green line. Channel depth noted and marked by $+++++$, along with approximate isodensity level and the chosen source thickness h_u shown inbetween.